

AC AND DC TRANSPORT IN ELECTROCHEMICALLY ETCHED POROUS SILICON LAYERS

*A Thesis Submitted in Partial Fulfilment of
the Requirements for the Degree of*
MASTER OF TECHNOLOGY

By
Joginder Singh

Material Science Programme
Indian Institute of Technology, Kanpur
June 1996

To

Aadi Sankara

And

Caitanya

14 OCT 1996
CENTRAL LIBRARY
I. I. T., KANPUR

Inv. No. A. 122318



A122318

MSP-1996-M-SIN-AC

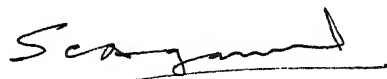
CERTIFICATE

This is to certify that the work presented in this thesis entitled, "AC AND DC TRANSPORT STUDIES ON ELECTROCHEMICALLY ETCHED POROUS SILICON LAYERS" by *Joginder Singh* is a record of work carried out under our supervision and it has not been submitted elsewhere for a degree.



(K. Shahi)

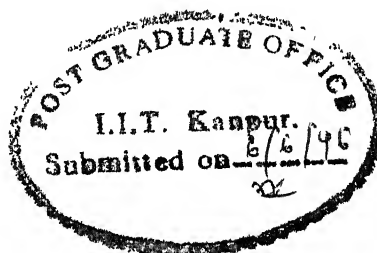
Materials Science Programme,
I.I.T., Kanpur.



(S. C. Agarwal)

Deptt. of Physics,
I.I.T., Kanpur.

June, 1996.



ABSTRACT

An electrolytic cell for preparation of porous silicon (PS) has been designed and fabricated. Using this cell, substrate-supported PS layers and free-standing PS layers are prepared by electrochemical etching of Boron doped crystalline silicon (c-Si) wafers. Preparation conditions have been established to obtain samples which show photoluminescence in the red-yellow region upon exposure to ultraviolet light from a mercury vapour lamp. I-V measurements are done in the temperature range $300K \leq T \leq 350K$, in sandwich as well as coplanar geometries. Both configurations give similar results. I-V characteristics are asymmetric in most cases and can be explained as transport limited by Poole-emission of carriers (Poole-Frenkel mechanism) or space charge limited currents (SCLC mechanism). In case of Poole-Frenkel mechanism, the data can be interpreted to give barrier heights of about 0.4–0.6eV which is in good agreement with the values reported in the literature. The dielectric constant calculated from the Poole-Frenkel fitting falls in the range 5–10. These values are similar to those published by other workers. Although I-V characteristics cannot be fitted to Poole-Frenkel mechanism in some cases, they can be fitted to the conduction by SCLC mechanism in all the samples. Using a step by step method for the SCLC mechanism, we calculate the density of states $g(E_f)$ at the Fermi level in the range $10^{16} - 10^{18} eV^{-1} cm^{-3}$.

ac conductivity measurements have also been done on PS at room temperature in the frequency range 5Hz–10MHz. The dielectric constant falls rapidly at low frequencies, say upto $\sim 5kHz$. It almost saturates to a constant value at high frequencies. The frequency dependence of the dielectric constant observed by us is same as reported in literature and has been explained accordingly. ac conductivity

σ_{ac} is found to be proportional to $\omega^{0.5}$ for low frequencies, say upto about $\sim 5\text{kHz}$. At higher frequencies, σ_{ac} increases almost linearly. The low frequency behaviour of σ_{ac} can be explained in terms of fractal properties of PS, with the random walk dimension $\sim 2.9 - 4.2$. The linear part of the frequency dependence of σ_{ac} at higher frequencies can be understood by assuming ac transport at the Fermi level. This gives the density of states at the Fermi level about $10^{17} - 10^{19} eV^{-1} cm^{-3}$. These values are in agreement with those found by other workers. The values of $g(E_f)$ obtained by ac and dc conductivity data are consistent with each other.

Acknowledgements

I pay my respects to Prof. S. C. Agarwal for introducing me to the fascinating field of semiconductor research and enabling me to produce ^{is} this piece of work under his inspiring and dedicated guidance. I am also indebted to Prof. K. Shahi for his meticulous and encouraging supervision towards this thesis and valuable advice from time to time. It has been thrilling to work with both of my supervisors.


I am thankful to Dr. Jitendra Kumar for allowing me to work in his lab for conductivity measurements and thermal evaporation of electrodes on my samples. I thank Dr. Satyendra Kumar for his caring and encouraging interaction.

My thanks are due also to my labmates Alokji, Anilji and Dr. Pratima Agarwal for their invaluable help in experiments and informal discussions. Subhashji and Madhukar are also thanked for the help they rendered during my experiments at ACMS. I am thankful to the wonderful company of Dr(s). G. S. Narayana, S. K. Tripathi and P. K. Dwivedi and their co-operation in all moments of lab-work. I also thank Ms Manju Malhotra, J. Singh and Manu Bajpai for all the smiles they radiated so lavishly.

The amount of effort that V. Ramesh and S. Pushpvanam put in the preparation of this manuscript outwits my attempts to thank them. Valuable suggestions of Shafi U. Khan and C. Ramesh in this regard are acknowledged. Thanks to George C. John for the bibliography database he lovingly contributed. I again thank Anilji for his advice regarding the shaping of this manuscript.

I am grateful to my friends Sushil, Venkat, Sangita, Kamal, Govind. Balvinder, Sundar, Sudipto, Subhasish, Giri and Ashutosh who made my four semesters a sweet

memory. I thank Sushil Raina especially for his philosophical expositions over hot cups of coffee and BTs. I shall also pay my respects to Dr. T. V. Prabhakar. Mataji (Mrs. Prabhakar) and Geeta Maa for their affectionate support at all times to which I owe the mental poise that was required during progress of this work.



(Joginder Singh)

Contents

1	Introduction	1
2	Experimental Details	9
2.1	Preparation of Sample	9
2.1.1	Substrate Preparation	10
2.1.2	Experimental set-up and Procedure	10
2.1.3	Free Standing Porous Silicon Layers	17
2.2	DC Measurements	19
2.2.1	Experimental Set-up and Procedure	19
2.3	AC Measurements	23
2.3.1	Experimental Set-up and Procedure	23
2.3.2	Measurement Details	24
3	Theory	26
3.1	DC Transport in Porous Silicon	26
3.1.1	Transport Limited by Poole-Frenkel Emission of Carriers	26
3.1.2	Transport Limited by Space Charge Limited Currents (SCLC)	28
3.2	AC Transport in Porous Silicon	31

3.2.1	Fluctuating Activation Energies and Pair Approximation . .	34
4	Results and Discussion	35
4.1	Experimental Results	35
4.1.1	Current-Voltage Characteristics	35
4.1.2	AC Conductivity Results	40
4.1.3	Capacitance and Dielectric Constant	44
4.2	dc Conuctivity–Discussion	47
4.2.1	Preliminaries	47
4.2.2	Poole-Frenkel Mechanism	48
4.2.3	Space Charge Limited Currents (SCLC)	52
4.2.4	AC Response of PS films	56
5	Summary and Conclusions	60
5.1	Scope for Future Work	63

List of Figures

- 2.1 Flow diagram of substrate preparation procedure.
- 2.2 Porous silicon formation set-up.
- 2.3 Cross-sectional view of teflon cell.
- 2.4 Teflon mask for selective area etching.
- 2.5 Lateral view of the brass electrode.
- 2.6 Nylon nut.
- 2.7 Lateral view of nylon seat.
- 2.8 DC conductivity measurement set-up.
- 2.9 Block diagram of dc conductivity measurement set-up.
- 2.10 AC conductivity measurement set-up.
- 2.11 Block diagram of ac conductivity measurement set-up.
- 3.1 Poole-Frenkel effect.
- 4.1 Time dependence of current (I) at 2V for PSL-7.
- 4.2 I-V characteristic of PSL-5 at room temperature.
- 4.3 I-V characteristic of PSL-5 at 343K.
- 4.4 I-V characteristics of PSL-5 in the temperature range 300–343K.
- 4.5 I-V characteristic of PSL-7 at room temperature.
- 4.6 I-V characteristic of PSL-7 at 343K.
- 4.7 I-V characteristic of PSL-7 in the temperature range 300–343K.
- 4.8 Frequency dependence of conductance at room temperature for PSL-5.
- 4.9 Frequency dependence of conductance at room temperature for PSL-7.
- 4.10 Frequency dependence of conductance at room temperature for PSL-8.
- 4.11 Frequency dependence of conductance at room temperature for PSL-9.

- 4.12 Frequency dependence of capacitance at room temperature for PSL-8.
- 4.13 Frequency dependence of capacitance at room temperature for PSL-5.
- 4.14 Frequency dependence of capacitance at room temperature for PSL-7.
- 4.15 Frequency dependence of capacitance at room temperature for PSL-9.
- 4.16 Poole-Frenkel plot for PSL-7.
- 4.17 Temperature dependence of zero-bias conductance (extrapolated) for PSL-7.
- 4.18 Bilogarithmic plot (for SCLC fit) of I vs V for PSL-7.
- 4.19 Temperature dependence of $(m-1)$ for PSL-7, PSL-10, PSL-11 and PSL-12.
- 4.20 Temperature dependence of $(m-1)$ for PSL-5.
- 4.21 Voltage dependence of dc current activation energy for PSL-7.

List of Tables

- 4.1 Preparation conditions of various samples.
- 4.2 AC conductivity data.
- 4.3 Parameters obtained from Poole-Frenkel fit.
- 4.4 Density of states ($g(E_f)$) obtained from SCLC fit.
- 4.5 Parameters calculated from ac conductivity data.

List of Symbols

ρ	dc resistivity.
σ	dc conductivity of porous silicon.
q	Electronic unit of charge.
k	Boltzmann constant.
T	Temperature in Kelvins.
d	Thickness of porous silicon film.
τ_d	Relaxation time of a carrier.
E_a	Current activation energy.
j	Current density.
$g(E)$	Density of states at an enegy level E .
ΔE_f	Fermi-level shift caused by a voltage step.
σ_{ac}	ac conductivity of porous silicon.
\bar{d}	Haussdorff dimension for a fractal.
\tilde{d}	Spectral dimension for a fractal.
d_w	Random walk dimension or diffusion exponent.
ξ	Correlation length.

Chapter 1

Introduction

The present decade has seen an explosion of research interest in Porous Silicon(PS). Although PS was discovered in 1956[1] it was the discovery of its photoluminescence (PL) in the red-yellow region, in 1990[2], which sparked off the present day interest in this material.

PS has been of relevance to research because of its scientific as well as technological prospects. The scientific challenge with PS is to unravel its formation mechanism, its microstructure as a function of preparation conditions and the origin of its visible photoluminescence at room temperature. An understanding of its electric and dielectric properties under a vast variety of conditions such as low and high temperatures, in vacuum and in presence of polar and non-polar media are among various other standard problems. Despite relentless efforts of various research groups these problems are still open-ended.

PS has been prepared by several methods of preparation. The first and most commonly used is the electrochemical etching of crystalline silicon (c-Si) in a dilute solution (about 25%) of HF and ethanol. Other methods, e.g., spark erosion[3, 4] and light induced etching of c-Si in HF[5, 6] have also been used but less frequently. In the

first method, a prepared substrate of doped (p- or n-type) c-Si is etched selectively with HF by passing a constant current across the interface of c-Si and electrolyte. If the substrate is doped n-type, it has been found necessary to illuminate it[7] during etching while a p-type substrate gives PS even if etched in dark. This is attributed to the role of holes in the etching process. A wide variety of PS layers with a host of pore morphologies and controllable thickness can be prepared using this method. The method can be augmented (by adding more steps) to prepare free-standing films of PS[8].

The discovery of photoluminescence in PS at room temperature in red–yellow region by Canham [2] marked the opening of a new field of research as it held the technological and scientific challenges both. The beginning of the present decade witnessed a tremendous amount of research seeking an explanation to the novel phenomenon of visible luminescence from Si—a base material for almost all electronic applications that remained unfit for opto-electronic devices so far. Bulk crystalline Si (c-Si) has both a relatively small and indirect energy gap which under normal circumstances prevents efficient interband radiative recombination. At room temperature c-Si shows a weak photoluminescence (PL) in the IR region at about 1.09 eV with a full width at half maximum (FWHM) that varies with excitation conditions but is typically $\sim 0.1\text{eV}$ [9, 10]. In contrast PS shows a strong PL at room temperature in the visible region at about 1.4–2eV with a comparatively narrow FWHM; the exact peak position for a particular sample depending upon the preparation conditions and post-etching chemical treatment[2, 11, 12, 13].

At Canham’s time, the structural aspects of PS were viewed in terms of crystallinity that deteriorates with increasing porosity thereby resulting in an amorphous phase [14]. He attributed the luminescence phenomenon to quantum confinement of electrons/holes in the Si columnar structures thus leading to band gap widening.

He based his arguments on simple Heisenberg principle of quantum mechanics to propose the valence band edge downshift and conduction band edge upshift.

Further experimental evidence for the above explanation was provided by early Raman studies on PS. Raman spectra on PS show low frequency side band which was attributed to a shorter coherence length of optical phonons in the direction perpendicular to the pore axis [15]. TEM studies also indicate the presence of quantum-size crystalline structure in PS [16]. Also, quantum-size effects have been invoked to explain the observation of visible luminescence in various systems containing silicon nanocrystals. which have been produced by techniques other than etching [17, 18, 19, 20, 21]. However, in 1992, Brandt et al [15] gave an alternative explanation now known as Siloxene model. They proposed that the visible luminescence in PS is not an intrinsic property of c-Si (quantum confinement effects) but depends upon the chemical reactions of silicon with hydrogen and oxygen thus bringing into importance the chemistry of pore formation which was not paid much heed by quantum confinement arguments as far as luminescence phenomenon was concerned. The support base for this proposition was a striking resemblance between the luminescent behaviour (life-times, intensities, positions. shifts etc.) of PS obtained by electrochemical etching and treated by a host of chemical processes and vibrational properties of Kautsky and Wohler[15] compounds obtained from siloxene.

Etching of PS performed with electrolyte containing a mixture of HF, HCl and Ethanol results in a luminescence band centred at 690 nm. This agrees well with the fluorescence of Kautsky siloxene annealed at 673K, the larger width in the latter case being due to rather uncontrolled substitution of hydrogen by OH groups during the annealing process. The red luminescence in PS obtained after etching in a solution of HF and Ethanol has a maximum at 760 nm. This luminescence agrees quantitatively

with the fluorescence of the Wohler compound after a similar annealing step at 673K. This agreement between the light emission from the PS on the one hand and the Kautsky and Wohler compounds on the other hand led Brandt et al to the siloxene model. This was further corroborated by infrared (IR) and Raman spectroscopies on these two types of materials[15].

Another model proposed for the mechanism of PL in PS was based on Si-hydride excitation [22]. The thesis put forward in this model is that etching process leads to the formation of Si-hydrides on the surface of PS and it is these hydride compounds which are responsible for the photoluminescence. The experimental basis for this proposition was the redshift and gradual disappearance of PL on annealing at temperatures in the range 503–663K. Prokes et al observed and argued in this paper that the pore widening treatments like chemical etching with HF do lead to blueshift in PL peaks. Earlier, Tsai et al [23] had made a headway in this approach by linking PL to hydride species. In this model, the peak position is located by distribution of hydrides and PL intensity is sensitive to the total surface area of PS layers[22].

It can be inferred from above statements that theory of photoluminescence (PL) of PS is still not established. Much activity in this direction is still going on to establish unambiguously the origin of PL in PS.

Apart from visible PL in PS, electroluminescence (EL) was also discovered[24, 25, 26]. This triggered an interest in the study of carrier transport in PS. In 1991, Halimaoui et al [24] found that liquid contacts on PS layers would operate as Light Emitting Devices (LEDs).

It was established in this way that solid, liquid and electropolymerised contacts on the PS layers exhibited electroluminescent properties[25, 26, 27]. Though PL efficiency was reported to be appreciable (up to 10%), the EL efficiency of LEDs referred

to above is disappointingly poor (only up to 0.01%). The theory of PL mechanism being incomplete, we need to work into the problem in order to understand the PL mechanism and to achieve efficient and stable optoelectronic devices. Thus, the transport studies in PS are worth undertaking due mainly to two reasons. Firstly, the PL is conditioned by radiative recombination of the non-equilibrium carriers and the photoconductivity is usually controlled by nonradiative recombination and so its study can help us to understand the PL mechanism as regards its microscopic origin. Secondly, an understanding of the transport of non-equilibrium carriers can give insight into the reasons for the low efficiency of PS-EL and thus an improvement of the same can be brought about. Owing to these reasons there is considerable attention being paid to the transport studies on PS at present.

The difficulties in the study of transport in PS are manifold. The nature of contacts that various metals and alloys thereof make on PS is not understood. For example, do the properties of the metal-PS contact depend upon the pore size, conductivity of the c-Si substrate, surface defects on PS and thickness of the film of PS? What are the factors leading to the best possible Ohmic or rectifying contact onto the PS? Next comes the question of transport mechanism itself. Is the transport by tunneling, hopping of carriers or band transport? Is transport isotropic, anisotropic, or what is the drift distance of the non-equilibrium carriers, comparable to or larger than the quantum size (2nm to 4nm)? Can the transport studies of transport give us some information about the micro (nano) structure of PS? Does the ageing of a sample of PS have an impact on results of transport phenomenon measurements? What are the magnitudes of time constants? The judging criterion for the transport studies, like any other study, is the coherence of its results with the established knowledge about PS and other studies on it. It is worth mentioning here that PS is not a well defined single material but represents a whole class

of materials. Microstructure can change from quantum wire columnar structure to oxidised (or otherwise passivated) partially connected spheres of silicon with thin tissue like material or even to thick, amorphous-like tissue with small embedded Si nanocrystals. This microstructure is a function of the substrate resistivity, porosity and can even change along the thickness of a particular sample of PS.

The reports in the literature in relation to transport studies can be classified into two main categories[28]. The first comprises of the cases in which the measured current density (in forward bias) at room temperature and at 1V is in the range of μA to mA per cm^2 [25, 29]. This is typical for PS with low porosity and (or) high conductivity substrates and (or) small PS thickness. The I-V characteristics in these cases are non-linear and diode-like over the entire range of applied voltages. This is explained as being caused by the resistances of electrode-PS interface, PS and PS-Si interface. The resistance of c-Si substrate is very low as compared to the other resistances in the series conceived above and can be neglected. In the cases above, the I-V characteristics are controlled by interfaces (Al-PS and PS-Si) and not the PS material[30]. The second category includes the cases with very low observed current densities ($\sim nA/cm^2$) at room temperature and 1V. The I-V characteristics in these cases are symmetrical and controlled by the conductivity of the PS material itself. This is typical for high porosity PS and (or) low conductivity substrate and (or) thick PS samples with strong PL[30, 31, 32]. In all of these above cases, PS layers and free-standing PS layers are grown on p-type c-Si substrates. Recently, investigations on free-standing PS layers grown from n+ substrates have been reported[33]. Diligenti et al in this reference observe a linear dependence of the current on voltage. The resistance of free-standing PS layers shows a thermally activated behaviour, with activation energies ranging from 0.1 to 0.44 eV which reduce upon decreasing the light intensity during anodisation of substrate. This can

be attributed to less porosity obtained for less intense illumination. However, they do not see any correlation between activation energy and anodisation current.

ac conductivity measurements[34, 35] have been extensively used to investigate both amorphous and glassy materials, as well as different ceramic and granular systems[36]. They allow one to investigate the broad range of relaxation times typical for nonhomogeneous and amorphous systems. In this way, it is possible to obtain more information on the underlying transport mechanism than from dc conductivity measurements alone. Ben-Chorin et al[37] employed this technique to understand the basic transport mechanism in PS and the reason for high resistivity of PS. On the basis of temperature-dependent ac measurements, they conclude that ac transport in PS is controlled by fractal geometry of PS at lower frequencies and by activated hopping at higher frequencies. ac conductivity scales to a power law dependence $\sigma(\omega) \sim \omega^s$ with s depending upon the frequency range selected. In the lower frequency range $s \simeq 0.5$ and in the higher frequency range $s \simeq 1$. They have modelled their scaling proposition using effective-medium approximation (EMA) for an activated hopping model on a percolating lattice.

The present study consists of ac as well as dc conductivity measurements on PS layers grown on c-Si substrates. The aim of these measurements is to find out the conduction mechanism prevailing during carrier transport in PS under the application of ac and dc fields.

The chapterwise plan of this study is as follows. Chapter 2 deals with the experimental details of the preparation of sample and the measurements performed. The design of the electrolytic cell used for PS preparation is described and also the experimental difficulties in the measurements are discussed. Carrier transport in PS is a problem of current interest and an elaborate work is in progress in the research on it. There are two main mechanisms proposed to operate, namely, the

Poole-emission of carriers from Coulomb traps and hopping around the Fermi level and the space charge limited current (SCLC) transport. The theoretical aspects of Poole-emission and SCLC are briefly described in Chapter 3. Chapter 4 presents the results obtained and possible explanations thereof using both the approaches. Finally, Chapter 5 gives the summary of our results and the conclusions drawn.

Chapter 2

Experimental Details

2.1 Preparation of Sample

Porous silicon (PS) has been prepared by several workers, mainly using three methods of preparation. First and most important is the electrochemical etching of crystalline silicon (c-Si) in a dilute solution of HF and ethanol. The other two methods are spark erosion [3, 4] and light induced etching of c-Si in HF [6, 5]. We prepared our samples by the first method in which a prepared substrate of doped (p or n) c-Si is etched selectively with HF by passing a constant current across the interface of c-Si and the electrolyte. If the substrate is n-type doped, it is necessary to illuminate it during etching while a p-type substrate gives PS even if etched in dark. This is attributed to the role of holes in pore formation[2, 7]. A wide variety of PS layers with a host of pore morphologies and controllable thickness can be prepared using this method. The same method can be augmented (by adding some more steps) to prepare free-standing films of PS[8].

2.1.1 Substrate Preparation

The substrate used is a p-type (Boron doped) polished c-Si wafer (resistivity (ρ) = $4 - 45 \Omega cm$, orientation $[100] \pm 5 \text{ deg}$). The wafer is cleaned chemically in a multistep process, as follows. First the wafer is boiled in trichloroethylene (TCE) to degrease and is rinsed with ethanol to remove residual TCE from it. The wafer is further cleaned in an ultrasonic cleaner, using acetone. The oxide layer on the crystal surface is removed by etching it with a dilute solution (20 %) of HF for about 30-40 secs. It is then rinsed with deionised water. The surface is found to be hydrophobic when it is clean. The metal film for back contact is aluminium and is evaporated thermally in vacuum ($\sim 10^{-5}$ torr), on the unpolished surface of c-Si wafer. Due to surface states and oxide layer developed on the surface during transfer into vacuum chamber, there develops a barrier across the silicon-aluminium interface. This makes the contact non-Ohmic. To overcome this problem, the silicon-aluminium system is annealed at $\sim 550 \text{ deg } C$ for about half an hour. At this temperature, alloying between the silicon and aluminium takes place at the interface and an Ohmic contact is achieved. c-Si with metal Ohmic back contact is the substrate for preparation of PS. This process is represented pictorially in Fig. 2.1.

2.1.2 Experimental set-up and Procedure

The electrolytic cell for preparation of PS was designed and fabricated as a part of the present work. The cell and its components are shown in Figs. 2.2-2.6. The cell consists of a Teflon cylinder in the middle of which a circular slot, coaxial with the cylinder, is engraved for fitting a mask in order to enable selective etching. The mask used is a Teflon disc with circular opening which is coaxial with the disc and the main cell. An O-ring is fitted inside a groove made around the central hole. This prevents the acid leakage as the substrate sits onto this O-ring during etching.

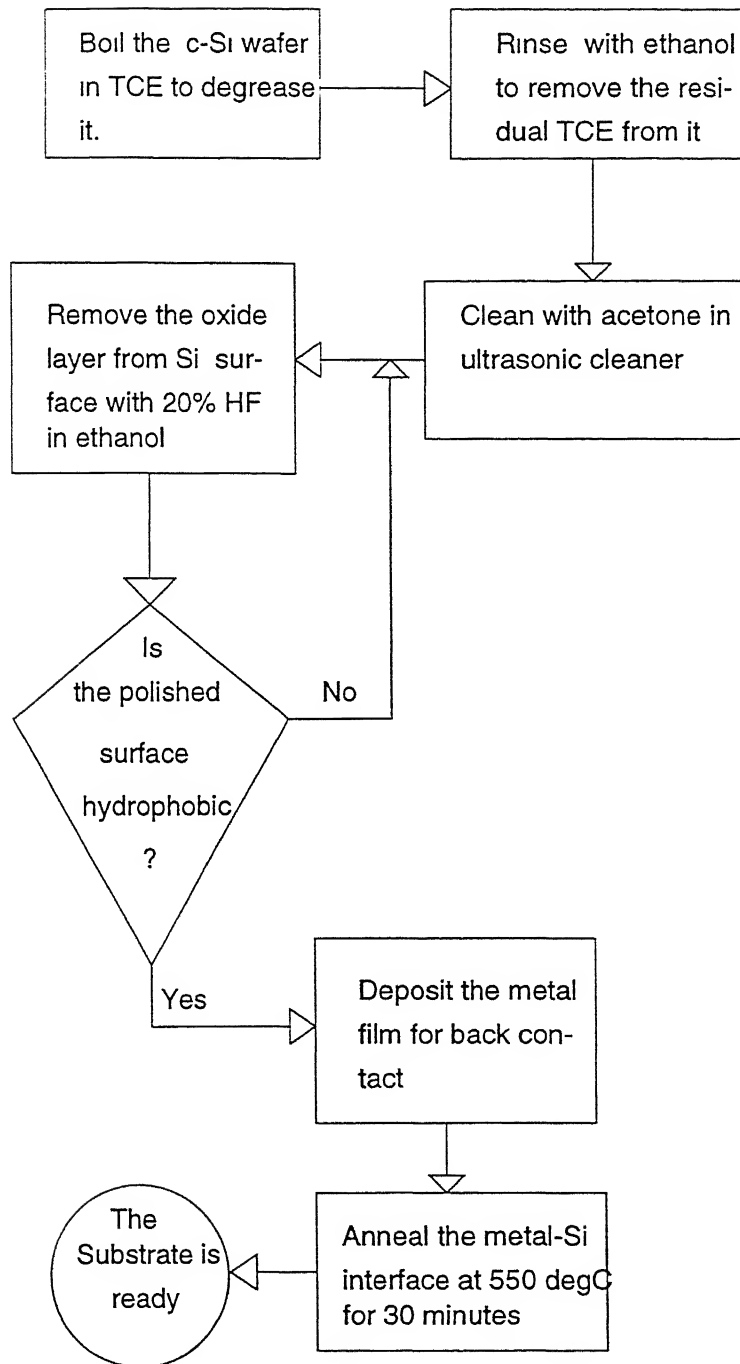


Fig. 2.1 Flow diagram for substrate preparation

The mask is placed on an O-ring put into the slot to ensure seal against acid leakage that can damage the cell structure. During etching, the substrate is placed onto the O-ring around the central opening in the mask with the face-to-be-etched in contact with it for selected area etching. The electrical contact for current flow is attained by the brass electrode placed onto the metal back contact on the substrate. The brass electrode is shown in Fig. 2.6 and is essentially a brass disc with a brass rod fitted coaxially into it. The surface of brass electrode in contact with metal film on c-Si is polished using emery paper for better electrical contact. Threads are made on the walls of Teflon cylinder inside this half into which fits a Nylon nut which has a through hole to accommodate the brass rod. By tightening the nut, optimum pressure can be put on the brass electrode to obtain good electrical connection between the c-Si substrate and the remainder of the circuitry. This arrangement is placed onto a Nylon seat with the polished face of the substrate turned up. The empty half of the cell serves as the electrolyte container. The Nylon seat is a hollow cylinder with a slot of same diameter as the outer diameter of the Teflon cell. The lower end of this cylinder is provided with a notch for leads to the remainder of the electrical circuit.

A 25% solution is prepared by adding 18 ml of 40% HF to 12 ml 99.9% ethanol. A Pt wire immersed into the electrolyte closes the circuit through power supply and voltmeter. A constant current is passed across the Si-electrolyte interface by anodising the c-Si substrate and Pt wire serves as cathode. Keithley 220 Programmable Current Source is used as the power supply and a Keithley 196 System DMM monitors the voltage drop across the c-Si-electrolyte system. The whole set-up is operated in a closed clean-bench provided with an exhaust fan. This provides a dust free environment to the experiment as also the hazards of HF fumes are averted by it.

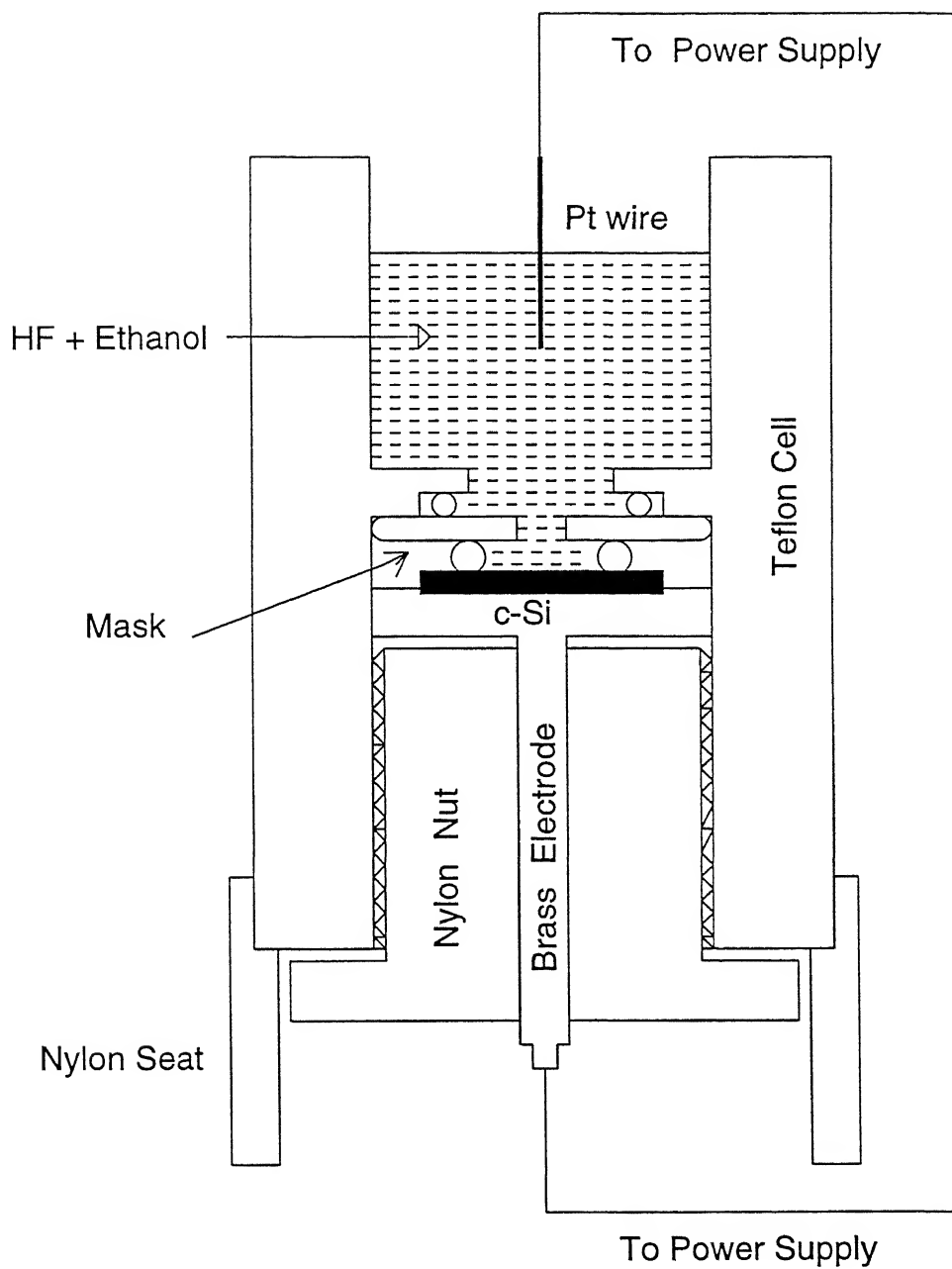


Fig. 2.2 Porous Silicon Formation Set-up

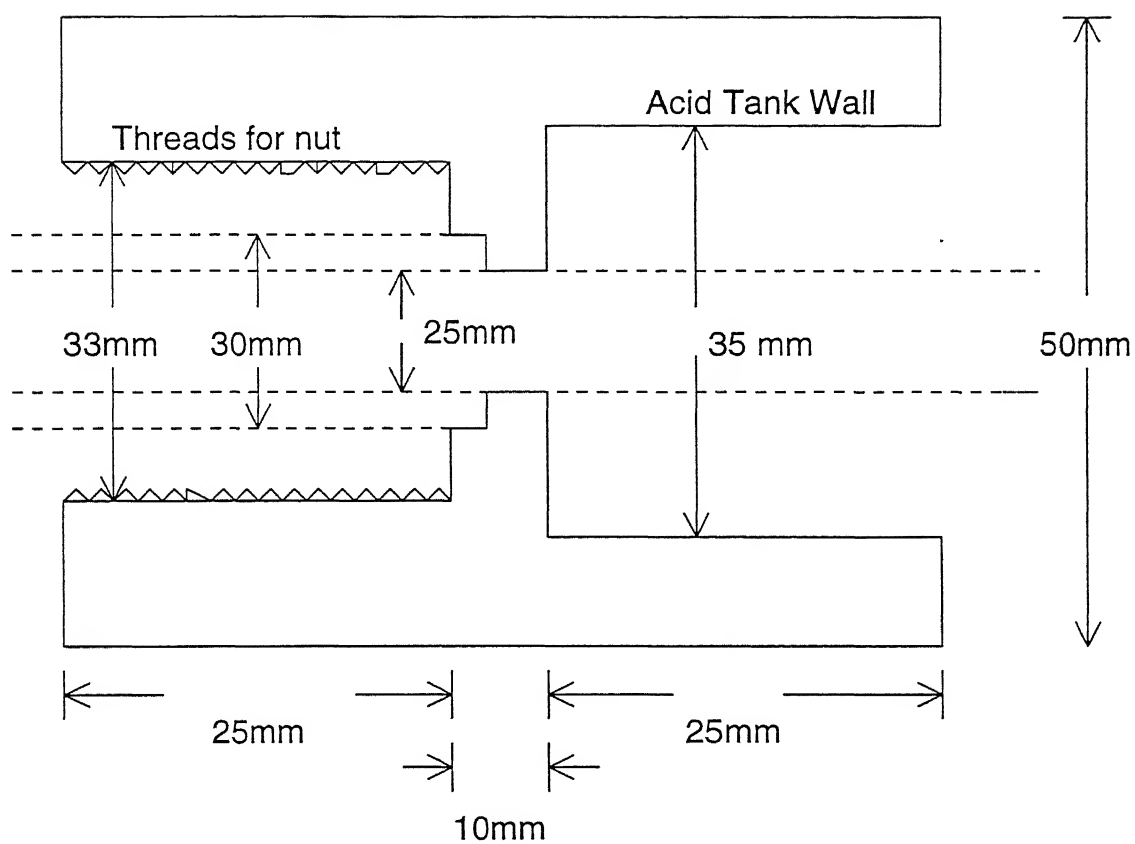


Fig. 2.3 Cross-sectional View of Teflon Cell

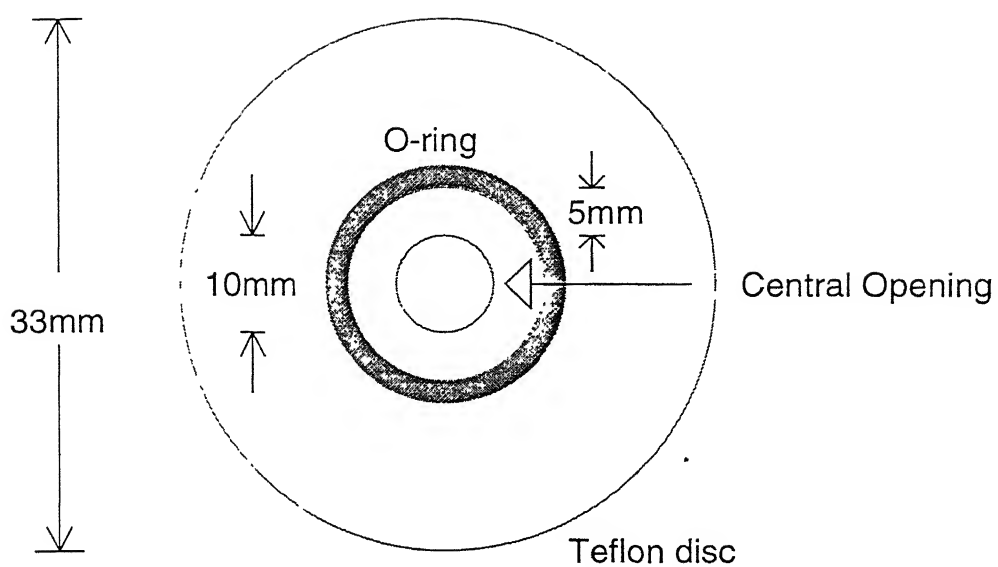


Fig. 2.4. Teflon Mask for Selective Area Etching

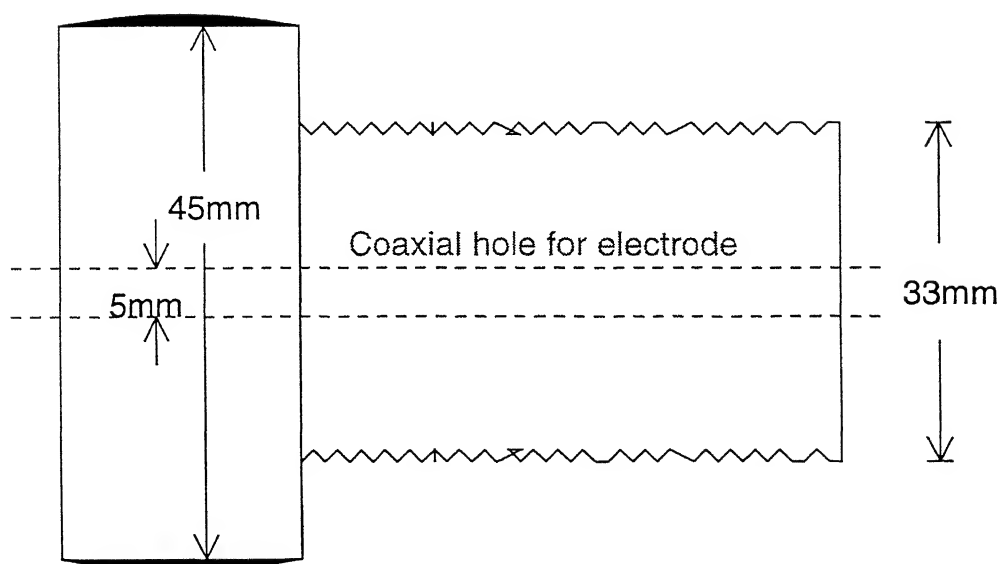


Fig. 2.5. Nylon nut

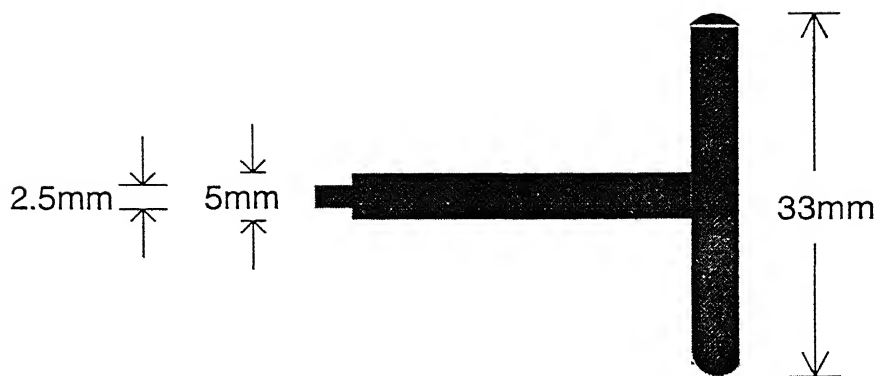


Fig. 2.6. Lateral View of the Brass Electrode
The Teflon Cell rests here

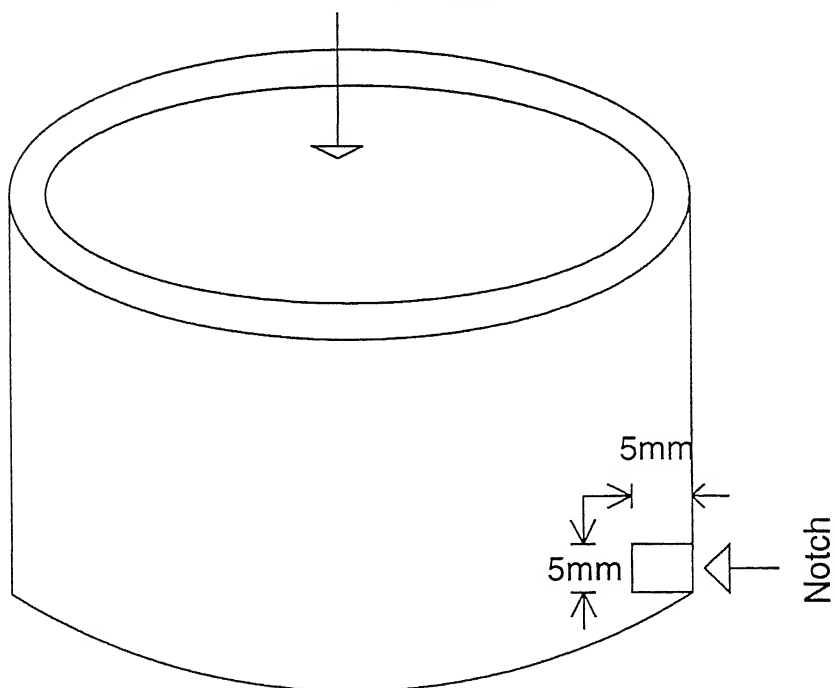


Fig. 2.7 A Lateral View of Nylon Seat

Initially, a high current (raising the current density to 300 mA/cm^2) is passed to electropolish the substrate for about 10 s. This makes the surface uniform for further etching. For a given etching and a concentration of HF, the etching time determines the thickness of the porous layer. The current source is programmed feeding it the etching (electropolishing) current, and the time for which etching should proceed, before turning the current on. As the etching progresses, bubbles start emerging from the substrate surface and go towards the cathode. Smith and Collins[38] attribute this to SiH_2 gas that evolves during pore formation.

After the etching is over, the electrolyte is removed from the cell and the cell is washed using de-ionised water ($10 \text{ M}\Omega$ resistance). The sample is rinsed with propanol and placed inside a vacuum chamber for drying at a roughing vacuum (10^{-2} torr) for about 30–45 minutes. The sample is then taken out for luminescence examination. A beam of uv light (from 125W Mercury lamp) is impinged onto the etched area. A typical sample luminesces red or yellowish red under uv illumination visible to the naked eye. The samples are stored in a desiccator in dark.

2.1.3 Free Standing Porous Silicon Layers

As reported in the literature, workers have primarily used three ways of preparing free standing films of PS. Firstly, Lee et al [39] report that all the other steps of PS preparation remaining the same as given earlier in this section, the etching current be increased gradually in small steps to its value for electropolishing. This dissolves the silicon below the initially formed PS layer uniformly instead of further pore formation and finally leads to dislodging of the PS film from the c-Si substrate. Second method by Lubianiker et al [40], consists of re-etching of PS layer for 5–6 minutes after electrochemical etching is over, by leaving sample standing in the electrolyte without passing any current through it. The third method is due to

Kanemitsu [8]. In this method, electrochemical etching of the substrate is carried out for 15–60 minutes depending upon the thickness desired and the current is abruptly raised to electropolishing value attaining a current density of about 700 mA/cm^2 . The free standing film of PS ($\sim 2 \times 3 \text{ mm}$) detaches from the c-Si substrate and can be collected using a spatula. We found that the first and the third methods give reproducible results and work for substrates of fairly wide ranging conductivity while the second method could not be reproduced for our substrates.

Initial attempts at preparing free-standing PS layers were fraught with many problems. A high etching current ($\sim 70 \text{ mA/cm}^2$ in our case) makes the film break into pieces immediately after it detaches from the substrate. Moreover, free-standing PS layers detach from the substrate with an impact which further aids the crumbling of the fragile films. This problem was overcome with etching current optimisation and increasing the etching time.

Etching for 5–20 minutes at 5 mA/cm^2 with 20% solution of HF and ethanol and increasing the current density to $300 - 500 \text{ mA/cm}^2$ abruptly did not lead to film separation. However, a weakly luminescent (red) PS layer was formed. The same process with high etching current ($\sim 70 - 80 \text{ mA/cm}^2$) also did not yield the free-standing PS layers. The PS layer formed in this case luminesces comparatively brighter. Etching for 40–60 minutes at a current density of 30 mA/cm^2 with 20% solution of HF and ethanol and subsequently increasing the current density to $\sim 550 \text{ mA/cm}^2$ in steps of about 20 mA/minute yielded a free-standing PS layer. This film was $\sim 2 \times 3 \text{ mm}$ in size and showed bright red luminescence. However, it was too fragile to facilitate any electrical measurements on it. Etching for the same time at a current density of 10 mA/cm^2 with the same solution for about one hour and flowing a current of 500 mA/cm^2 for $\sim 5-10$ minutes yielded a free-standing PS layer of $2 \times 3 \text{ mm}$ size. This film was robust enough to withstand the pressures of the

electrical contacts put during measurements. Photothermal deflection spectroscopy (PDS) on this sample showed it to have crystallites of size $\sim 3.5nm$.

2.2 DC Measurements

2.2.1 Experimental Set-up and Procedure

Al or NiCr contacts were evaporated thermally onto the PS layers in an oil diffusion pumped vacuum system having a base pressure of $\sim 10^{-6}$ torr. Since the surface of the material is porous, the vapours of the metal to be deposited onto the PS surface may enter into the pores. In case the pores extend to the crystalline substrate, which has considerably higher conductivity than PS, the penetration of the metal down to the bottom may lead to short-circuiting. To avoid this, the samples were kept in slanting position during evaporation so that vapours impinge on the PS surface at an angle of $\sim 60 - 75$ deg. Circular dots of 1-2 mm dia were evaporated onto PS layer using stainless steel masks. I-V measurements were performed on these metal-PS-Si trilayers in sandwich as well as coplanar configurations. As the surface of a particular PS film is rough due to dislodging of atoms from it during etching, an intimate contact cannot be attained between the probe and the metal dot by applying pressure as it may damage the structure itself. In order to avoid this difficulty, Indium pads were kept between the probe and the dot on the PS surface. The experimental set-up used for the measurements of I-V characteristics of PS structures is as shown in Fig 2.8. A thin mica sheet is mounted on a copper block fixed inside the vacuum chamber using silver paint. The sample is stuck onto the mica sheet again using silver paint. The I-V characteristics are measured in sandwich and coplanar geometries using Keithley 617 electrometer. The current at each applied voltage decreases initially for a few seconds and then stabilises.

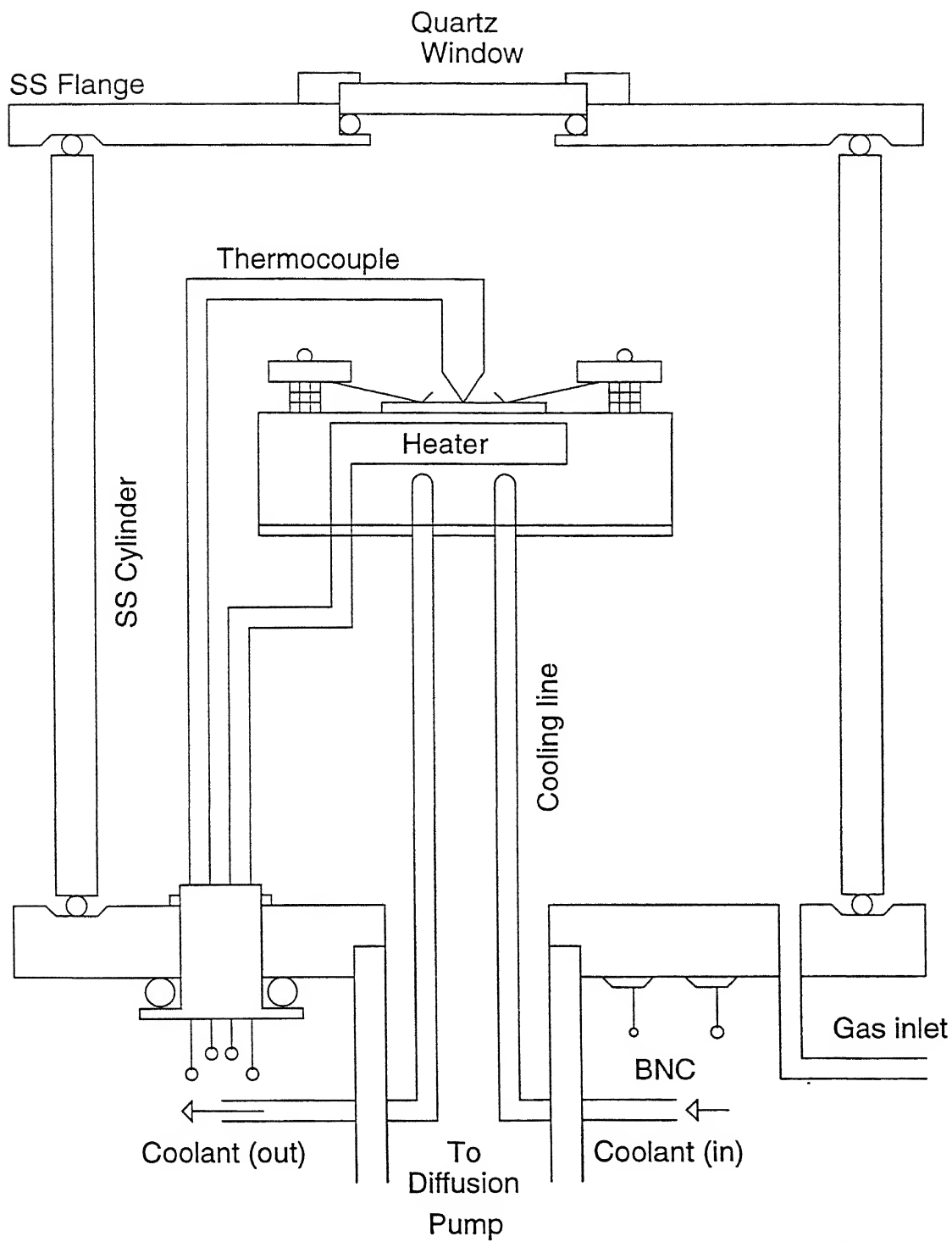


Fig. 2.8. DC Conductivity Measurement Setup

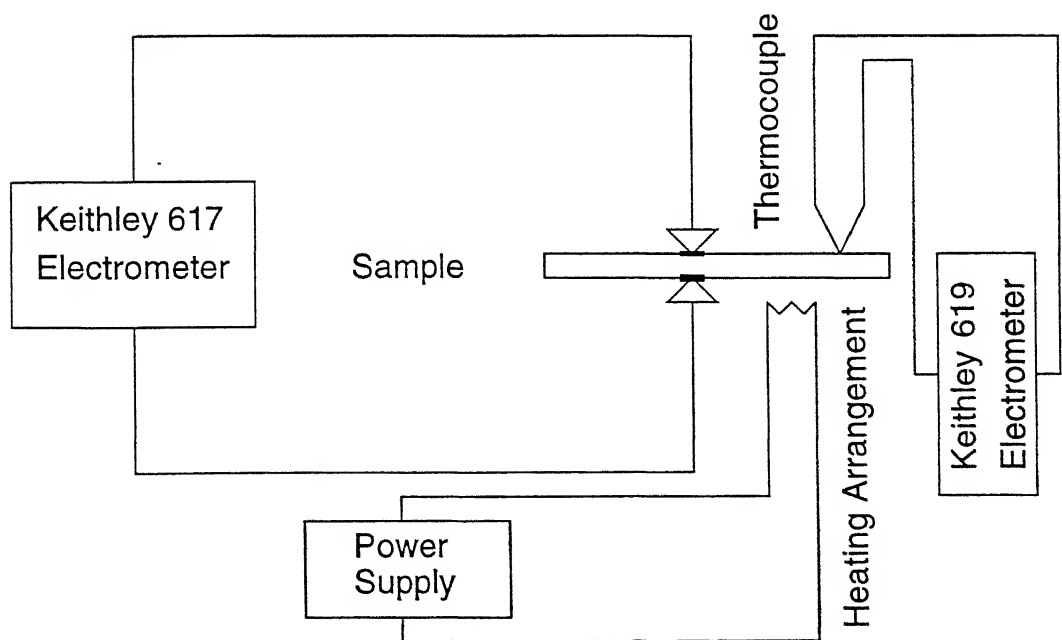
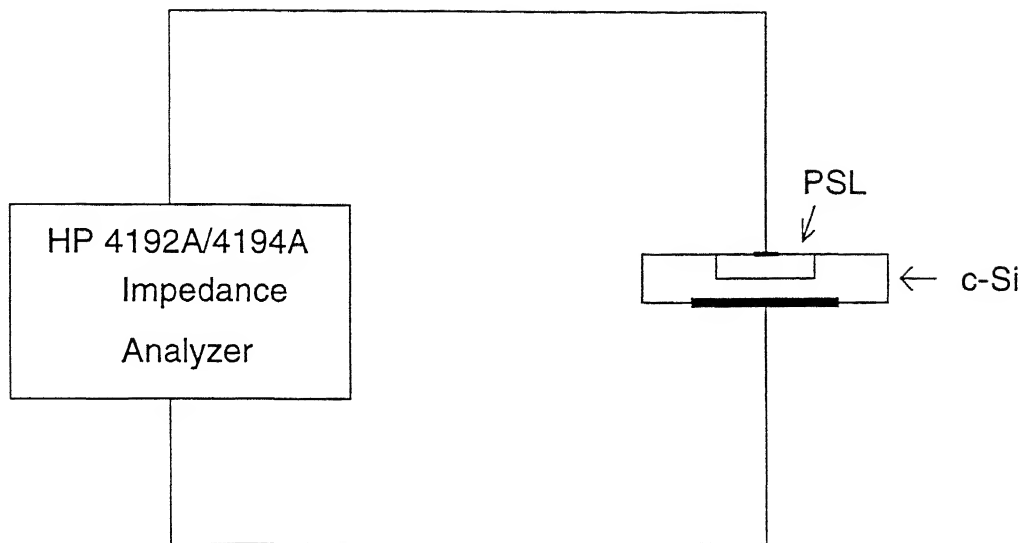


Fig. 2.9 Block Diagrams of σ_{ac} and dc Conductivity Measurement Set-ups

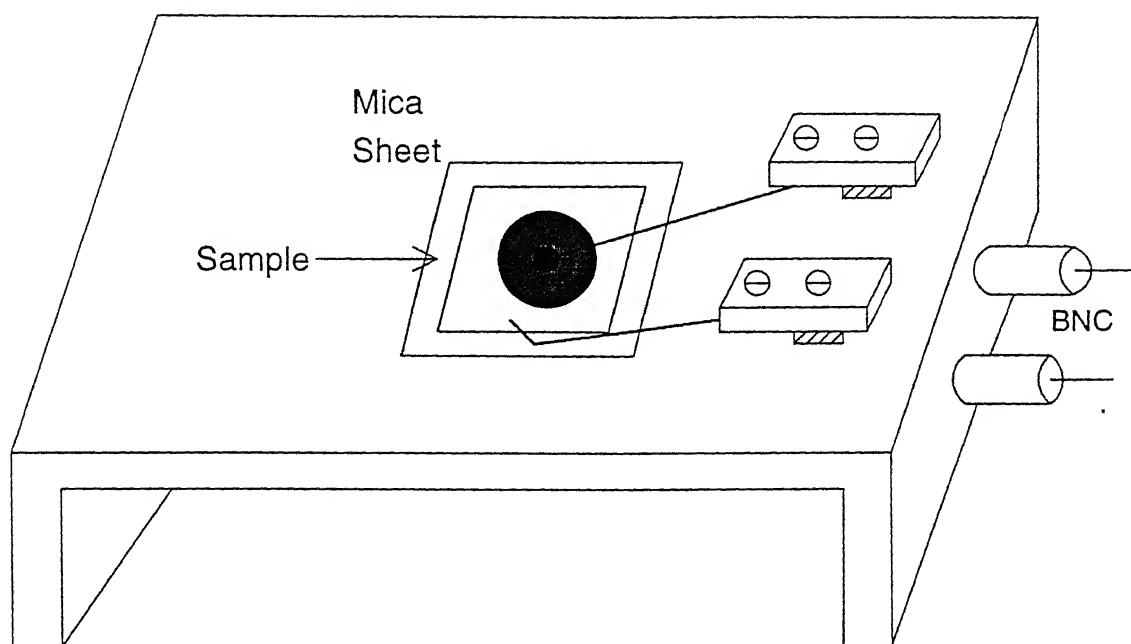


Fig. 2.10 Sample Holder for ac Conductivity Measurement

Therefore, a certain delay time is kept between the application of the voltage and detection of current for each of the sample at each temperature case specifically. A particular delay time is chosen for an I-V run so that the change of the current at a particular voltage is limited to the second place of decimal and thus current is stable to the first decimal digit. These delay times are in the range 10-100 s. The copper blocks are connected to heater leads from a regulated dc power supply and the temperature of the sample can be changed. A Copper-Constantan thermocouple mounted on a nearby dummy sample was used to measure the temperature of the sample for each I-V run. Fig 2.9 shows the block diagram of the circuit.

2.3 AC Measurements

2.3.1 Experimental Set-up and Procedure

The set-up used for ac conductivity measurements is as shown in Fig. 2.10. Two copper probes are fitted onto an aluminium platform through brass blocks. These blocks are electrically insulated from the aluminium base using teflon washers. The pressure that a particular probe puts on the PS film can be controlled by turning the fine screw arrangement provided for the purpose. The whole set-up is enclosed in an aluminium box to avoid noise. The ac measurements of sample conductance (G), susceptance (B) and capacitance (C) are made using HP 4192A and HP 4194A Impedance Analyzers in the frequency range 5 Hz to 10 MHz. Each of these bridges has a four probe configuration with standard lead length of 1m. The measurements are made in two terminal configuration by shorting the source measurement leads to voltage source leads. The oscillation level applied across the sample was in the range 50 mV to 1V. Under such conditions, a low ac signal is passed through the material and it avoids thereby the irreversible electrode changes and heating effects. As the measurements are done over a wide frequency range, the various polarisation processes occurring in the sample may be resolved.

Fig. 2.9 shows block diagram of ac conductivity measurement set-up. The principle of ac measurement is as follows. The Impedance Analyzer, operated in parallel mode, measures the conductance (G) and susceptance (B) components of admittance (Y). The rest of impedance parameters like capacitance (C) etc., are then calculated from these two by the computation routines in the Impedance Analyzer itself.

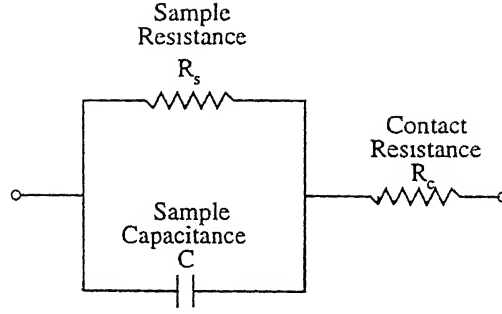


Fig. 2.11. Equivalent circuit for ac conductivity measurement

2.3.2 Measurement Details

As pointed out in the previous section, we go for the admittance measurements thereby measuring the conductance (G) and susceptance (B) assuming an equivalent circuit as shown in Fig. 2.11. These are selected from four general representations, viz., impedance (Z), admittance (Y), permittivity (ϵ) and modulus (M) spectroscopies. Since a variety of relaxation processes with differing relaxation times are expected in porous silicon (PS), the choice is obvious as they furnish ready information without much assumptions that should be made for calculating parameters from the observed data. The relationships between the components of admittance and permittivity are given as under

$$Y = G + jB \quad (2.1)$$

$$\text{or } Y = G + j\omega C \quad (2.2)$$

$$\text{or } Y = j\omega\epsilon C_0 \quad (2.3)$$

$$\text{and } \epsilon = \epsilon' + j\epsilon'' \quad (2.4)$$

$$\text{or } \epsilon' = \frac{B(\omega)}{\omega C_0} \quad (2.5)$$

$$\text{and } \epsilon'' = \frac{G(\omega)}{\omega C_0} \quad (2.6)$$

$$\text{Also, } \sigma(\omega) = \epsilon_0 \omega \epsilon'' \quad (2.7)$$

$$\text{and } \sigma(\omega) = \frac{\epsilon_0 G(\omega)}{C_0} \quad (2.8)$$

where C is the capacitance of the sandwich structure of the sample PS, $C_0 = \epsilon_0 A_c / \ell$ is the vacuum capacitance of the empty measuring cell of electrode area A_c and electrode separation ℓ and $\sigma(\omega) = G(\omega) \ell / A_c$ is ac conductivity of PS.

Chapter 3

Theory

3.1 DC Transport in Porous Silicon

In the literature, the dc transport in PS has been described in terms of Poole-Frenkel emission of carriers from Coulombic traps and space charge limited currents (SCLC)[30, 41]. We describe the salient features of the theory of these two mechanisms.

3.1.1 Transport Limited by Poole-Frenkel Emission of Carriers

It is generally observed that insulators and semi-conductors display, in high electric fields E (over 10^6 volts/cm for the former and a few thousand volts/cm for the latter), an increase of electrical conductivity which finally leads to breakdown. This field dependance can be represented by $\sigma = \sigma_0 \exp(\alpha E)$ called Poole's law. The fact that the illumination of an ^electronic semi-conductor increases its conductivity independent of E can be used to infer that the increase of the electrical conductivity

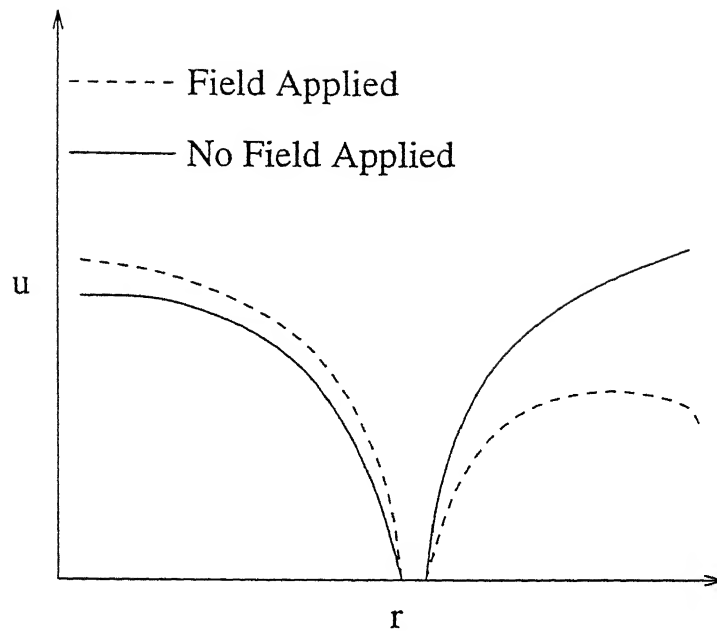


Fig. 3.1 Poole-Frenkel Effect.

in intense fields is due to the increase of the number of free electrons and not of their mobility

Frenkel[42] sought to explain this behaviour viewing a dielectric material not as a system of free electrons moving in a self-consistent periodic field of force, but simply as a system of neutral atoms. This refers to the normal state in which there are no free electrons. After the ionisation of an atom, the electron can be viewed as moving freely in the surrounding medium consisting of neutral polarisable atoms and in the field of remaining positive ion. Since this field is screened by the polarisation of the surrounding atoms, the ionisation energy must decrease. In an external field E , this energy is further decreased by a mechanism similar to that of Schottky effect in the thermoelectric emission from metals. In Fig. 3.1, the full line represents the potential energy of the electron as a function of the distance from the positive ion

while the dotted line represents the same quantity in the presence of the field. The height of potential barrier is lowered in the field by

$$\Delta\phi = qEr_0 + q^2/\epsilon r_0 \quad (3.1)$$

where r_0 , the distance to the maximum from the ion, is given by $q^2/\epsilon E$. Thus, $\Delta\phi = 2q\sqrt{(eE/\epsilon)}$. Assuming the number of free electrons due to thermal ionisation of atoms is proportional to $\exp(-\phi_0/2kT)$, electrical conductivity in presence of field is proportional to $\exp(-(\phi_0 - \Delta\phi)/2kT)$.

We thus obtain

$$\sigma = \sigma_0 \exp(\sqrt{(q^3 V/\epsilon \pi d)}/kT) \quad (3.2)$$

Where V is the applied voltage and d is the thickness of sample. This is Frenkel-Poole equation. It is interesting to note that on the basis of the above theory the effect of field is reduced by elevation of temperature.

3.1.2 Transport Limited by Space Charge Limited Currents (SCLC)

The current injected by a metal contact into the insulator/semi-conductor is controlled by the contact if the injection is weak. If contact is sufficiently injecting, there builds up a space charge region inside the insulator and resists the further injection of carriers. Under such conditions, the currents are controlled by the space charge. An ideal ohmic contact is an infinite reservoir of carriers and zero voltage drop occurs across the metal-insulator interface. In other words, the electric field strength should be enough to equalise the transit time to the relaxation time. If the applied voltage is smaller than that required to fulfill above condition, the injected carriers are redistributed maintaining thereby the charge neutrality. In this ohmic region,

the current is proportional to the first power of the applied voltage. For SCLC conduction to occur, the applied voltage should be higher than the critical one required to reduce the transit time (t_t) below relaxation time (τ_d), i.e., the injected excess free charge carrier concentration dominates the equilibrium, thermally generated charge carrier concentration.

Owing to defects and admixtures which are present in the material which may act as traps, the injected charge is redistributed in these traps and changes τ_d , so that the condition $t_t = \tau_d$ is again valid and a new steady state value of the current is achieved. In practice, however pure SCLC condition of infinitely injecting contact is not achievable. The charge carrier injection from the electrode takes place, modified, for example, by thermionic emission, field emission, thermionic field emission or surface states etc. and the electrical transport through the sample is then influenced by the contact. Both the concentration of free carriers and the magnitude of the current depend on the degree of filling of the trapping centres, as well as on the voltage applied. Thus, I-V measurements could be used for energy-trap distribution.

The activation energy E_a of the current on applied voltage is defined [43] by the relation

$$E_a = -\frac{d(\ln j)}{d(1/kT)} \quad (3.3)$$

By plotting E_a versus applied voltage, we can arrive at the distribution of density of trap-states. SCLC approach is usually employed to estimate the density of states (DOS) function $g(E)$ for trap states [44]. For an exponential energy-trap distribution of type $g(E) = g_0 \exp(-(E - E_f)/kT_0)$ a power law dependence of current on applied voltage of the form

$$I = C \frac{V^m}{d^{2m-1}} \quad (3.4)$$

where d is the sample thickness and C is a constant.

For any particular sample of thin film, d is a constant. The value of the exponent m can be obtained as slope of the straight line region in a plot of $\log(I)$ against $\log(V)$. Another test for above calculations to be accurate is the temperature dependence of $(m - 1)$. $m - 1 = T_0/T$ for exponential DOS distribution. Thus, a plot of $m - 1$ versus $1/T$ should be a straight line passing through origin. If DOS distribution is not exponential above technique cannot be employed.

In this context, the method suggested by denBoer [45] seems more plausible for DOS calculation. In this method, although the spatial variation in the DOS is neglected, no particular distribution in energy is assumed, a priori. A voltage step $\Delta V = V_2 - V_1$ shifts the quasi Fermi-level (E_f) by an amount

$$\Delta E_f = kT \ln(I_2 V_1 / I_1 V_2) \quad (3.5)$$

Assuming that all the charge goes to traps, the total charge injected per unit area by a voltage step ΔV is

$$\begin{aligned} Q_t &= \frac{\epsilon \Delta V}{d} \\ \text{or } Q_t &= qd \int_{E_f}^{E_f + \Delta E_f} g(E) dE \\ \text{or } Q_t &= qd g(E) \Delta E_f \end{aligned}$$

The assumption that $g(E)$ is constant within the limits of integration holds for small enough voltage steps. From above equations, we arrive at

$$g(E) = \frac{\epsilon \Delta V}{qd^2 \Delta E_f} \quad (3.6)$$

3.2 AC Transport in Porous Silicon

Usually, the hopping transport between localised states is the reason for frequency dependance of the conductivity. The disorder results in a wide distribution of hopping rates and gives a strong dispersion of ac conductivity. In most of the systems investigated, the real part σ_{ac} of complex dynamic conductivity $\sigma(\omega)$ has a frequency dependence

$$\sigma_{ac} \propto \omega^s \quad (3.7)$$

with $s \simeq 1$. This frequency dependance relates a small dc conductivity to a high local one which (with increasing frequency) is due to the polarisation of increasingly small conducting units. Though such behaviour of ac conductivity is ubiquitous in disordered materials, it can have different microscopic origins [37]. For electronic transport, the relevant mechanisms are electron localisation with associated hopping [46] and fractal topology [47]

Ben-Chorin et al [37] have proposed a theoretical formulation of the problem leading to a scaling law in both the cases basing their approach on random walk of carriers on a fractal network under the influence of impressed ac signal. The details of the derivation can be found in the reference quoted above. Assuming that ac response is due to the diffusive motion of carriers with charge q , the complex dynamic conductivity $\sigma(\omega)$ is given by the generalised Einstein relation

$$\sigma(\omega) = q^2 \frac{\partial n}{\partial \mu} D(\omega) \quad (3.8)$$

Here $D(\omega)$ is the generalised frequency-dependant diffusivity, n the number of carriers and μ the chemical potential ¹.

¹For non-interacting carriers in the case of Boltzmann statistics, we have $\partial n / \partial \mu = n / kT$, and for Fermi statistics $\partial n / \partial \mu = g(E_f)$, where $g(E_f)$ is the density of states at the Fermi-level

For non-interacting carriers the diffusive motion of the carriers is described by a single-particle random walk. *Normal diffusion* is the case if mean square distance walked by the particle increases linearly with time, i.e.,

$$\langle r^2(t) \rangle = 6Dt \quad (3.9)$$

where D is Diffusion coefficient independent of frequency. *Anomalous diffusion* is present if it increases sublinearly with t , for example, according to

$$\langle r^2(t) \rangle \propto t^{2/d_W} \quad (3.10)$$

where $d_W > 2$ is the *random walk dimension or diffusion exponent*. This implies an anomalous frequency-dependant conductivity of the form $\sigma(\omega) \propto (\omega)^s$ with $s = 1 - 2/d_W$. A crossover from $\omega^{1/2}$ dependence to linear dependence on ω of real part of complex dynamic conductivity is equivalent to transition from anomalous diffusion for times $t < t_0$ to normal diffusion for $t > t_0$.

A fractal [48] is a self similiar geometrical object in which the mass M of a region of diameter L scales as $M(L) \propto L^{\bar{d}}$, $\bar{d} < d$, where d is the dimension of the embedding space and \bar{d} is the *Haussdorff or fractal dimension*. The x-ray (or neutron) scattering intensity of materials with fractal properties varies with wave number q as $i(q) \propto q^{-\bar{d}}$. In fact, such anomalous small-angle scattering has been observed for PS [49, 50].

It has been shown by Alexander and Orbach that a random [37] walk on a fractal implies a sublinear time dependence $\langle r^2(t) \rangle \propto t^{2/d_W}$ with

$$d_W = 2\bar{d}/\tilde{d} \quad (3.11)$$

where \tilde{d} is the spectral or fracton dimension, and we have $\tilde{d} < \bar{d}$. The fracton dimension is determined by the vibrational density of states $g(\omega)$ of the fractal which

is proportional to $\omega^{\bar{d}-1}$. Accordingly the temperature dependence of the specific heat is given by $C(T) \propto T^{\bar{d}}$.

An example of a fractal which has been studied extensively by numerical and analytical theoretical work is a percolating lattice [51] . In the bond percolation problem, impurities are distributed at random with concentration x and are treated as connected if they occupy nearest-neighbor sites. In both cases, below a critical concentration x_c only connected clusters with finite size exist. At a critical concentration x_c an infinite cluster appears which is percolation cluster. For $d = 3$ it has a fractal dimension $\bar{d} \simeq 2.5$ and a spectral dimension $\tilde{d} \simeq 1.33$. This gives the random walk dimension as $d_W \simeq 3.77$ and correspondingly $s \simeq 0.47$. d_W has also been determined independently by numerical simulation [51] to be in the range $3.45 \leq d_W \leq 4.0$. These numbers apply both for site and for band percolation.

In percolating systems, the presence of finite clusters even for $x > x_c$ leads to a slightly larger value of s as compared to that given by the relation $s = 1 - 2/d_W$ [52] . Since we are not dealing with a percolating system, but with a porous material, which is more similar to the backbone of the infinite percolation cluster and does not contain isolated clusters of material, this effect can be neglected.

For $x > x_c$, one can define a correlation length ξ . On length scales smaller than ξ the structure of the percolating network looks like the critical cluster, on a scale larger than ξ it looks homogeneous. The concept of correlation length can be generalised. Consider a system which on length scales smaller than ξ has fractal properties and on length scales larger than ξ is homogeneous. The mean square distance in such a system behaves as

$$\begin{aligned} \langle r^2(t) \rangle &= 6Dt_0(t/t_0)^{2/d_W} \text{ for } t \ll t_0 \\ \text{and } \langle r^2(t) \rangle &= 6Dt \text{ for } t \gg t_0 \end{aligned}$$

The correlation length is defined now as

$$\xi = \sqrt{(Dt_0)} \quad (3.12)$$

Porous Si is such a system, because on a macroscopic scale it is homogeneous.

3.2.1 Fluctuating Activation Energies and Pair Approximation

Let us assume that r_{ij} is the separation between two sites i and j with an activation barrier E_{ij} . The hopping probability per unit time is assumed to be of the form

$$W_{ij} = \nu_0 \exp(-E_{ij}/kT) \quad (3.13)$$

where ν_0 is attempt frequency. For classical barrier hopping, ν_0 should be of the order of a phonon frequency $\nu_p \sim 10^{12}$ Hz. For phonon-assisted tunneling between localised states, there is additional tunneling factor $\nu_0 = \nu_p \exp(-2r_{ij}/\tilde{\xi})$, where $\tilde{\xi}$ is the localisation length [37]. Ben-Chorin and coworkers in this reference have applied pair approximation to this process. In this approximation, the carriers are assumed to hop between isolated pairs of sites. The frequency dependent diffusivity is given by

$$D(\omega) \simeq \langle r_{ij}^2 [1/W_{ij} + 1/i\omega]^{-1} \rangle \quad (3.14)$$

where $\langle \rangle$ means an average over large number of pair configurations. Proceeding in this way and assuming a uniform barrier distribution we obtain for ac conductivity in the frequency regime $\omega \ll \nu_0$ [46]

$$\sigma'(\omega) = q^2 a^5 N^2(E_f) kT \omega \pi / 2 \quad (3.15)$$

Chapter 4

Results and Discussion

4.1 Experimental Results

4.1.1 Current-Voltage Characteristics

On the basis of our measurements, we classify our samples of PS in two main categories; one has asymmetric diode-like I-V characteristics and the other has more or less symmetric I-V characteristics with respect to the polarity of the applied voltage. Fig. 4.1 shows the time dependence of current measured at an applied voltage of $2V$ at $300K$ for PSL-7. The preparation conditions for this and other PS samples are given in Table 4.1.

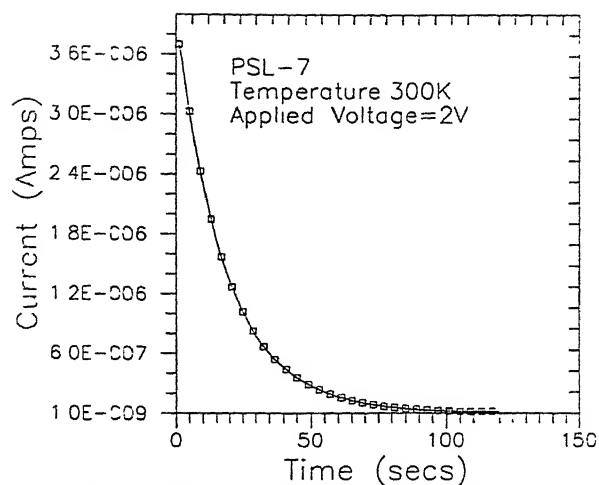


Fig 4.1. Time dependence of current i on cooled voltage 2V

Table 4.1. Preparation Conditions of PS samples

Sample Name	Substrate $\rho(\Omega cm)$	Etching Current (mA/cm ²)	Etching Time (min.)
PSL-5	4-45	20	15
PSL-6	4-45	10	15
PSL-7	4-45	20	45
PSL-8	4-45	5	15
PSL-9	4-45	70	30
PSL-10	4-45	50	30
PSL-11	4-45	30	30
PSL-12	4-45	20	30

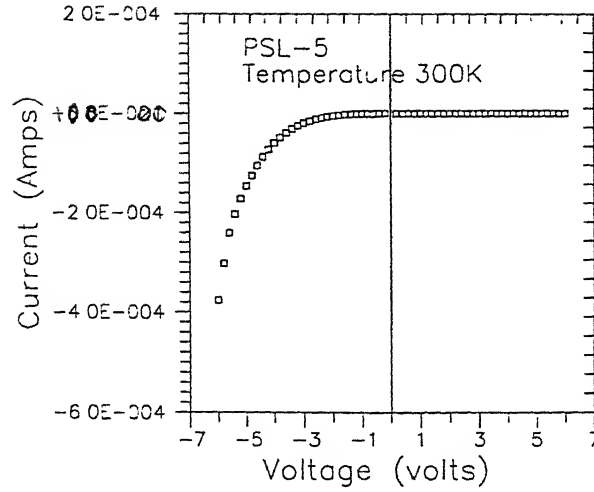


Fig. 4.2 I-V characteristics of PSL-5 at room temperature

Fig. 4.2 shows a plot of current versus voltage taken at room temperature for PSL-5. Negative sign with the voltage signifies that Al dot on PS is negative and the positive sign of voltage is for source positive connected to the Al dot. The I-V characteristics have a diode-like form; the trilayer Al-PS-Si is forward biased when Al dot is negative. The forward bias has two sub-regions. For applied voltages (V_{app}) between zero and $-3V$, the I-V curve is sub-Ohmic while for more negative values ($V_{app} \leq -4V$), it exhibits a super-Ohmic behaviour. Fig. 4.3 shows the I-V characteristics for the same PS sample in the same voltage range but at a higher temperature (343K). It may be noted that the super-Ohmic behaviour begins for voltages more negative than $-2V$. The sub-Ohmic region is restricted between zero and $-1V$. From these two figures as also from Fig. 4.4, we conclude that the transition from sub-Ohmic to super-Ohmic region is sensitive to temperature of the measurement. Higher the temperature, lower is the magnitude of bias at which the transition takes place.

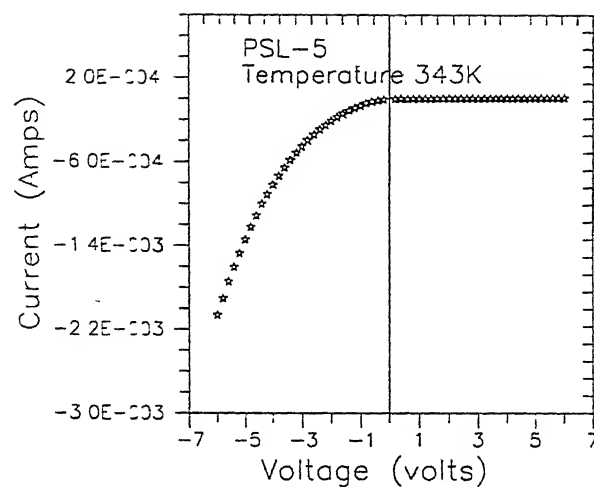


Fig. 3 I-V characteristics of PSL-5 at 343K

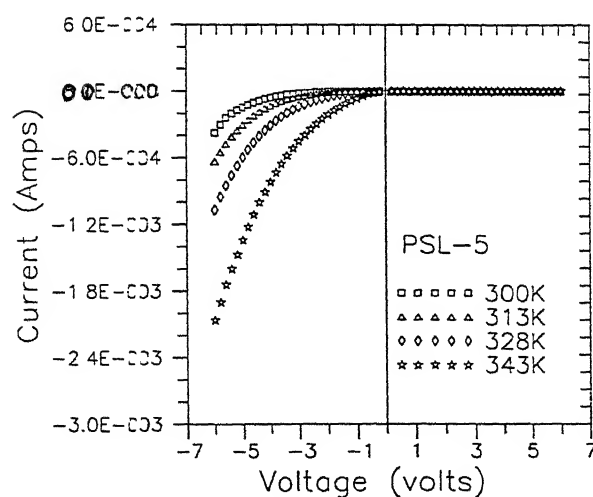


Fig. 4 I-V characteristics of PSL-5 in the temperature range 300-343K.

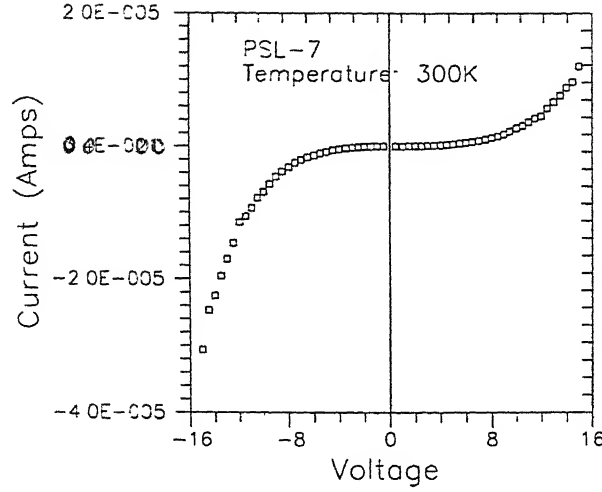


Fig. 4.5. I-V characteristics of PSL-7 at room temperature

Figs. 4.5 and 4.6 show I-V characteristics for PSL-7 at 300K and 343K respectively. The I-Vs are super-Ohmic at voltages more negative than $-8V$ and sub-Ohmic from $-8V$ to zero bias. In the range of positive voltages, the sub-Ohmic region for $0 < V_{app} < 8V$ makes a transition to super-Ohmic region ($V_{app} > 12V$). That these regions are sensitive to temperature changes is clearly seen by comparison of Figs. 4.5 and 4.6. Fig. 4.7 further confirms this observation. Above results can be summarised as follows. The I-V characteristics of all PS samples at all temperatures have two non-Ohmic regions; a sub-Ohmic region at lower voltages and a super-Ohmic region at higher voltages. The exact value of voltage demarcating the two regions varies from sample to sample, i.e., on preparation conditions like etching time and etching current. For a particular sample, the extent of one of the two regions is influenced by temperature. At higher temperatures, the samples exhibit a super-Ohmic behaviour over the entire voltage range.

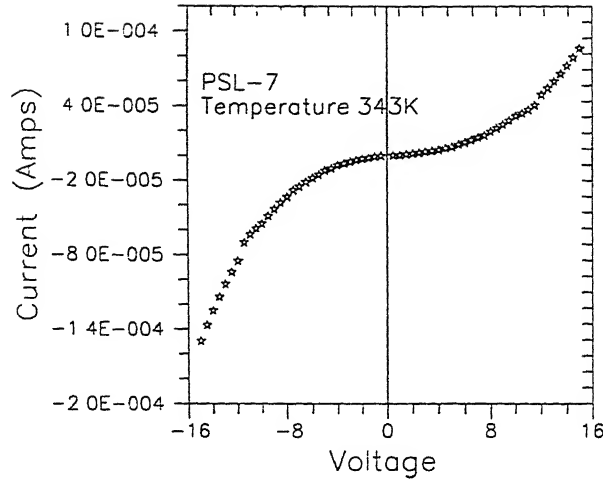


Fig 4.6 I-V characteristics of PSL-7 at 343K

4.1.2 AC Conductivity Results

In Fig. 4.8, ac conductance (G) is plotted against frequency for PSL-5 in the frequency range 10 Hz to 10 MHz at room temperature. The applied oscillation level is fixed at $1V_{rms}$ and no dc bias is applied. The conductance undergoes a change of about three orders of magnitude from $3.3 \times 10^{-8}S$ to $7.5 \times 10^{-5}S$ in the measured frequency range. The figure indicates that the frequency response of conductance has two regions. In the lower frequency range ($10 \text{ Hz} < \omega < 10 \text{ kHz}$), the power law $\sigma_{ac} \propto \omega^s$ is obeyed with $s \simeq 0.38$, and the upper limit on frequency range is not very sharply defined for this region. In the frequency range above this fuzzy limit, the exponent $s \simeq 1$. The power law fit straight lines intersect at $\omega_c = 41 \text{ kHz}$. The extrapolated value for zero frequency conductance is about $0.033\mu S$ which is far above the dc conductance ($\sim 10^{-9} \frac{S}{\mu m}$). Thus, in the employed range of frequency, the ac conductivity does not saturate to the corresponding dc value for the sample.

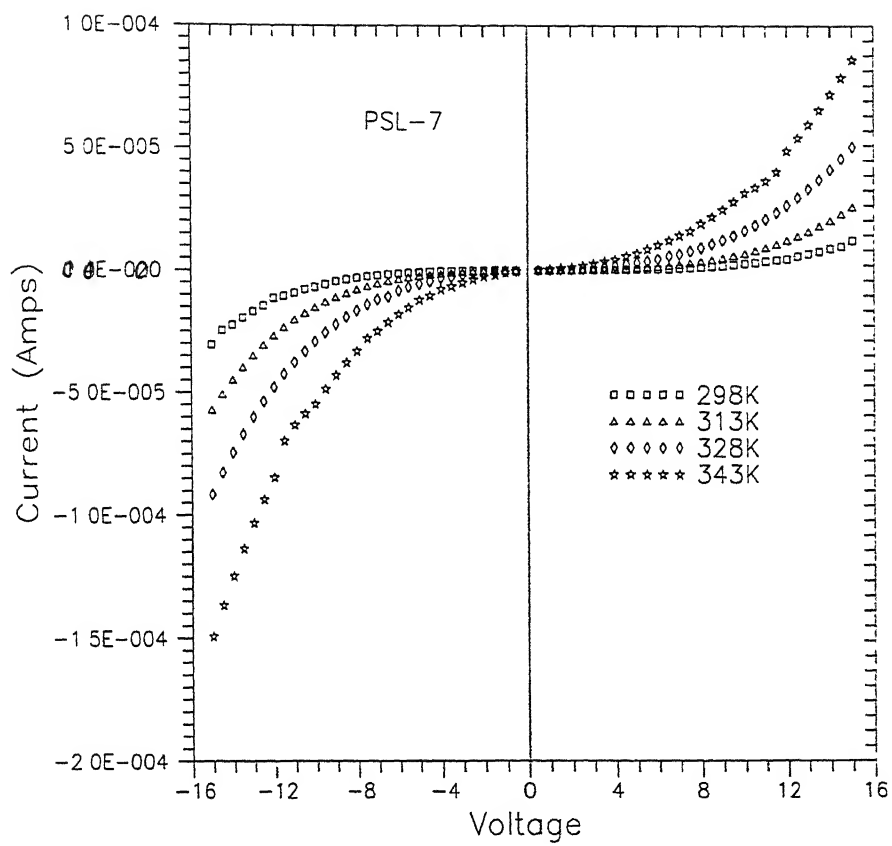


Fig 4.7 I-V characteristics of PSL-7
in the temperature range 300-343K

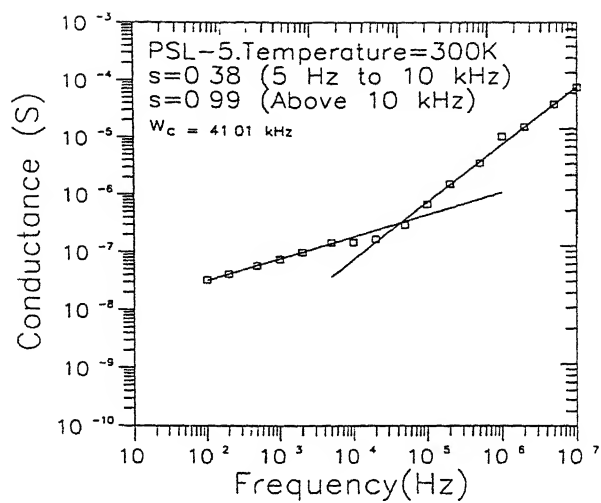


Fig. 4.8. ac conductance of PSL-5 as a function of frequency at 300K.

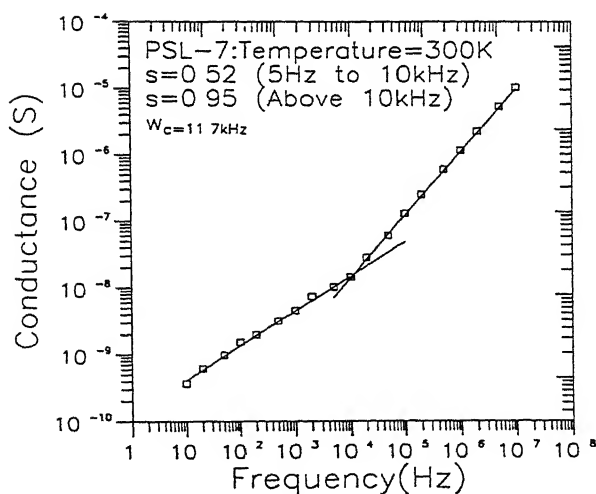


Fig. 4.9. ac conductance of PSL-7 as a function of frequency at 300K.

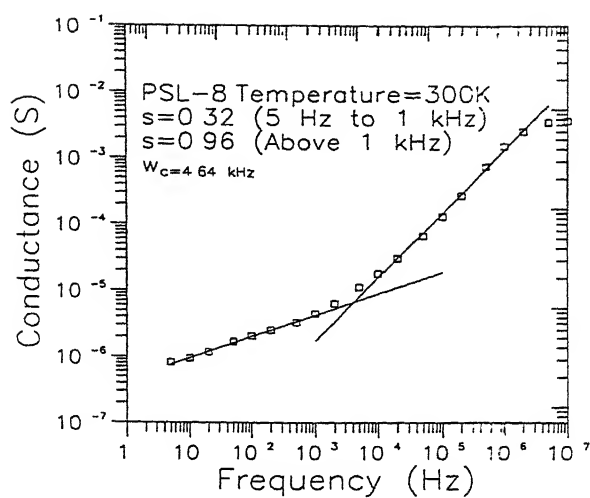


Fig. 4.10 ac conductance of PSL-8 as a function of frequency at 300K

Similar results are obtained for other samples too (cf. Figs. 4.9 – 4.11). These results are summarised in Table 4.2.

Table 4.2. ac conductivity data of PS films

Sample Name	Exponent s		ω_c (kHz)
	Low Frequency	High Frequency	
	Range	Range	
PSL-5	0.38	0.99	41
PSL-7	0.52	0.95	12
PSL-8	0.32	0.96	5
PSL-9	0.51	0.98	29

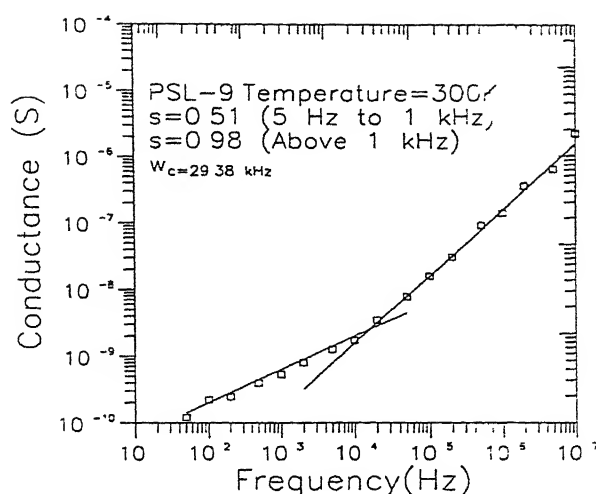


Fig. 4.11 ac conductance of PSL-9 as a function of frequency at 300K

4.1.3 Capacitance and Dielectric Constant

Fig. 4.12 represents frequency dependence of capacitance for PSL-8 at room temperature in the frequency range 10 Hz to 10 MHz at zero dc bias. The details of the sample preparation conditions can be seen in Table 4.1. As seen in the figure, the frequency response of the capacitance has also two distinguishable regions as regards the rate of variation of capacitance. In the lower frequency range (10Hz to about 100Hz), the capacitance falls from 10.6 nF to about 1.6 nF . At higher frequencies, the capacitance changes only slightly from less than 1.6 nF at 100 Hz to $\sim 0.2\text{ nF}$ at 10 MHz . The rapid fall in the low frequency range and near saturation attainment at higher frequencies is noteworthy. Similar behaviour is observed in other samples too (cf. Figs. 4.13–4.15).

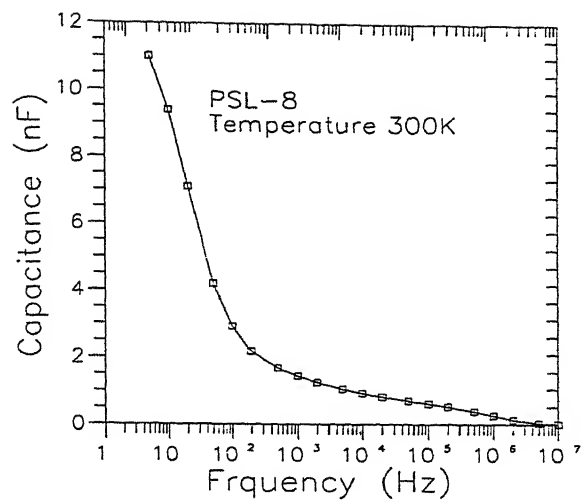


Fig. 4 12 Capacitance of PSL-8 as a function of frequency at 300K

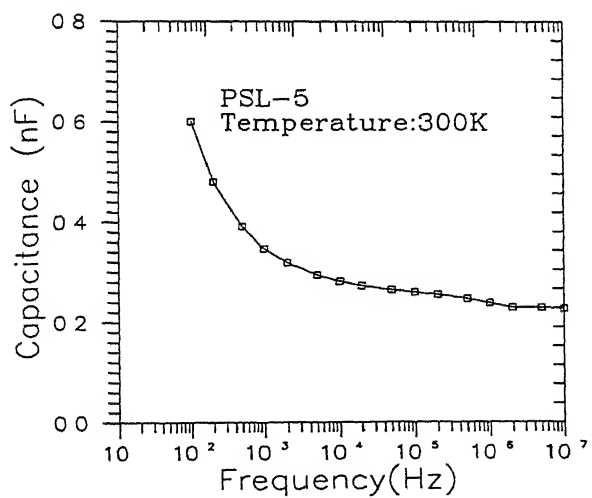


Fig. 4 13 Capacitance of PSL-5 as a function of frequency at 300K.

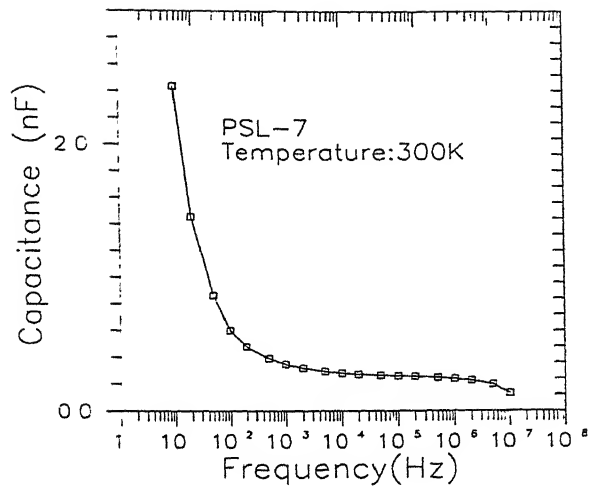


Fig. 4.14 Capacitance of PSL-7 as a function of frequency at 300K.

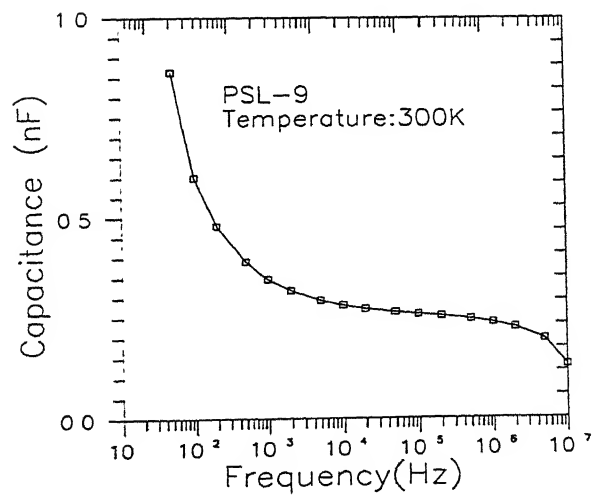


Fig. 4.15 Capacitance of PSL-9 as a function of frequency at 300K.

4.2 dc Conuctivity–Discussion

4.2.1 Preliminaries

As remarked in the beginning of this chapter, we classify our observations in two main groups. The first group comprises of those on samples for which I-V characteristics are asymmetric with respect to the polarity of applied voltage. One example of this category is PSL-5 for which the current density at 1V is $8.45 \times 10^{-5} A/cm^2$ at room temperature . The I-V characteristics for this sample are diode-like and hence the transport is controlled primarily by the contacts between the Al-dot and PS as well as PS-Si interface. Such a behaviour is attributed to low porosity of PS or small thickness thereof ($< 1\mu m$)[28, 30].

The trilayer Al-PS-Si can be understood qualitatively as a series combination of voltage-dependent resistance (of PS) and a rectifying barrier(s). The rectifying barrier may be formed by the Al-PS contact, PS-Si interface or both of them. If the porosity of PS is low, it has low resistivity and hence contact resistance gives rise to the asymmetric I-V behaviour as observed. Or otherwise, if the PS layer is thin enough ($< 1\mu m$) it has a low resistance effectively and again the current is controlled by ~~the~~ contact resistance. Low porosity PS samples are non-luminescent or luminesce very feebly[53]. Since PSL-5 has bright red luminescence, it is a high porosity sample. Probably effective thickness of PS film is small.

The second group comprises of samples with I-V characteristics symmetric with respect to polarity of applied voltage. Thus, the I-V behaviour in this category of samples is independent of nature of contact on PS and is limited by the resistance of PS. This may be due to high porosity of PS or enough thickness thereof.

The reports in literature[30, 41] argue that the transport in PS can be understood in terms of Poole-Frenkel or SCLC (space charge limited currents) mechanisms.

4.2 dc Conductivity–Discussion

4.2.1 Preliminaries

As remarked in the beginning of this chapter, we classify our observations in two main groups. The first group comprises of those on samples for which I-V characteristics are asymmetric with respect to the polarity of applied voltage. One example of this category is PSL-5 for which the current density at 1V is $8.45 \times 10^{-5} A/cm^2$ at room temperature . The I-V characteristics for this sample are diode-like and hence the transport is controlled primarily by the contacts between the Al-dot and PS as well as PS-Si interface. Such a behaviour is attributed to low porosity of PS or small thickness thereof ($< 1\mu m$)[28, 30].

The trilayer Al-PS-Si can be understood qualitatively as a series combination of voltage-dependent resistance (of PS) and a rectifying barrier(s). The rectifying barrier may be formed by the Al-PS contact, PS-Si interface or both of them. If the porosity of PS is low, it has low resistivity and hence contact resistance gives rise to the asymmetric I-V behaviour as observed. Or otherwise, if the PS layer is thin enough ($< 1\mu m$) it has a low resistance effectively and again the current is controlled by ~~the~~ contact resistance. Low porosity PS samples are non-luminescent or luminesce very feebly[53]. Since PSL-5 has bright red luminescence, it is a high porosity sample. Probably effective thickness of PS film is small.

The second group comprises of samples with I-V characteristics symmetric with respect to polarity of applied voltage. Thus, the I-V behaviour in this category of samples is independent of nature of contact on PS and is limited by the resistance of PS. This may be due to high porosity of PS or enough thickness thereof.

The reports in literature[30, 41] argue that the transport in PS can be understood in terms of Poole-Frenkel or SCLC (space charge limited currents) mechanisms.

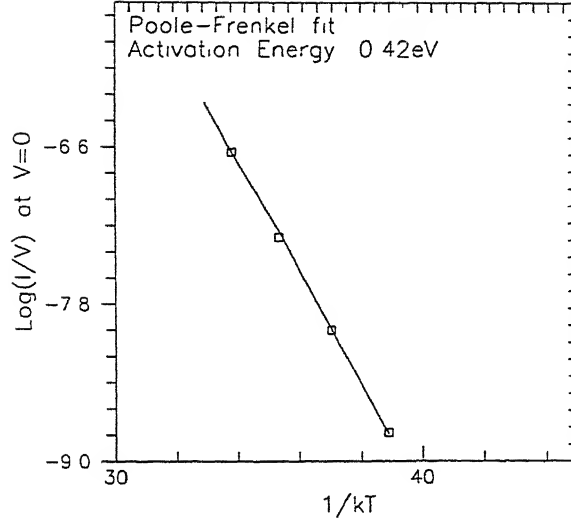


Fig. 4.17 Temperature dependence of zero bias conductance (extrapolated) of PSL-7

over the entire range of applied voltages for reasons that will be touched upon later in this section. However, linear regions in each curve satisfy the equation

$$G(V, T) = G_0 \exp(\beta\sqrt{V} - \phi_0/kT) \quad (4.1)$$

where $\beta = (q^3/(\pi\epsilon d))^{1/2} \lambda^{-1/2}$ as derived in §3.1.1. This suggests the Poole-Frenkel relation that applies for transport via electric-field-enhanced thermal excitation of carriers from Coulomb traps[42]. Fitting a straight line in the linear region and extrapolating it to intersect the conductance axis, we obtain the set of values of zero bias conductance at each temperature. These values obey a linear dependence on $1/T$ in semi-logarithmic plot as shown in Fig. 4.17. The slope of this line gives the activation energy ϕ_0 of $0.55 \pm 0.04\text{eV}$. The activation energies for Poole-emission from Coulombic traps calculated for various samples are given in Table 4.3.

Table 4.3. Parameters obtained from Poole-Frenkel fit

Sample	$\phi_b(\text{eV})$		Dielectric Constant	Remarks on I-V relation
	-ive bias	+ive bias		
PSL-5	0.55	–	5.36	Asymmetric
PSL-7	0.39	0.42	8.52	Symmetric
PSL-9	0.60	–	7.67	Asymmetric
PSL-10	–	–	–	Symmetric
PSL-11	0.57	0.52	10.21	Symmetric
PSL-12	0.13	0.16	6.56	Asymmetric

Tables 4.1 and 4.3 seem to suggest certain trends in the activation energy as a function of preparation conditions. Too high etching current (as in PSL-9) creates deeper traps and the depth of these traps reduces as the etching current is lowered down (PSL-11, PSL-12). Etching time sets no trend in the dc activation energy of PS. This can be linked with the depletion of carriers in the etching process. More etching means almost elimination of the shallow level carriers and in such a case, only deep level traps can influence the current conduction. Another test on Poole-Frenkel mechanism is performed by seeing the reasonability of parameters calculated from the last equation. As $\epsilon = \epsilon_0 K$, we have

$$\beta = (q^3 / (\pi \epsilon_0 K d))^{1/2} 1/kT \quad (4.2)$$

This equation can be used to obtain dielectric constant of PS. Table 4.3 lists the dielectric constants obtained from Poole-Frenkel fit for various samples. It is obtained by optical experiments employing shape-dependent effective medium averaging over regions of the order of few μm . For transport in Poole-Frenkel sense,

a local electric field on the scale of few tens of angstroms is relevant. These dimensions are comparable to crystallite sizes reported for PS in the literature [32, 30]. For such crystallites, the notion of dielectric constant does not apply. As a consequence, K obtained from this fitting does not reflect directly any physical feature of the material and should be viewed as a fit parameter only.

The exponential dependence of conductance on \sqrt{V} could also be brought about by carrier injection over Schottky barrier at the contacts when the screening length is much larger than the film thickness [54]. However, Schottky emission depends on the barrier heights at the metallic contact and at the PS-Si substrate interface. It must lead to asymmetric dependence of G on V with respect to the polarity of applied voltage. Since the barrier heights at the two interfaces are not same as is observed for those samples which exhibit asymmetric I-V behaviour. It stands in contradiction to what is being presented in the present context.

From a comparison of electron-microscopy data with computer models [38] as well as small-angle X-ray [49, 50] scattering, it is known that PS network of crystallites has a fractal structure. A strict application of the Poole-Frenkel mechanism per se to this system is not reasonable. For this mode of conduction, the current is carried by charges which are thermally excited from traps to some transport band. The simple \sqrt{V} dependence applies only for Coulombic traps and the granular structure of PS on the angstroms scale disturbs the electric field distribution at the trapping site. Moreover, disorder in PS does not allow the excited carriers to move freely as is assumed in the simple Poole-Frenkel model. Disorder can be incorporated into the model following the work of Pai [55]. He assumed that the excited carriers diffuse by Brownian motion under the influence of long range field of the coulomb-center and showed theoretically that the conductivity will have the same temperature dependence and a very similar field dependence to that predicted

by the simple Poole-Frenkel case. The reason for this is that carriers move a long way under the coulombic potential before they are able to escape and thus the details of short range disorder do not affect the general behaviour. An escape of a carrier from a trap-state occurs when it reaches a critical distance R_c from the Coulombic centre. for which the thermal energy kT is larger than the Coulombic energy, $q^2/\epsilon_0 K R_c$. For room temperature, R_c can be as large as 1000\AA [30] and for higher temperatures it will be shorter. Since this length scale is much larger than that of the porous structure, it is not surprising that the experimental results may be fitted using an effective dielectric constant.

4.2.3 Space Charge Limited Currents (SCLC)

Although Ben-chorin et al [30] negate the possibility of SCLC mechanism in their samples of PS, as they do not observe any super-Ohmic region in their measurements, Kocka et al [41] stress its probability in their experiments on free standing films of PS. The clear super-Ohmic regions in the I-V characteristics observed in our samples (cf.Figs. 4.2–4.7) supports the hypothesis put forward by Kocka et al[41]. In pursuit of fitting SCLC mechanism to our data, we plot $\log(I)$ versus $\log(V)$ for PSL-7 in the temperature range 298-343K in Fig. 4.18. As pointed out in Chapter 3, an exponential energy trap distribution leads to a power law dependence of current on voltage of type $I = kV^m$. Slope of linear region, in the bilogarithmic plot of I-V, which is not linear over entire voltage range, in Fig. 4.18 gives the exponent m . Further, $m - 1 = T_0/T$. In none of our samples we observe that the plot of $m - 1$ versus $1/T$ is a straight line passing through origin (cf.Fig. 4.19). In a couple of samples, for example in PSL-5 (cf Fig. 4.20), $m - 1$ versus $1/T$ has linear behaviour but the straight lines are far from passing through the origin. In a majority of our samples (cf. Fig. 4.19), we see that the $m - 1$ versus $1/T$ plots

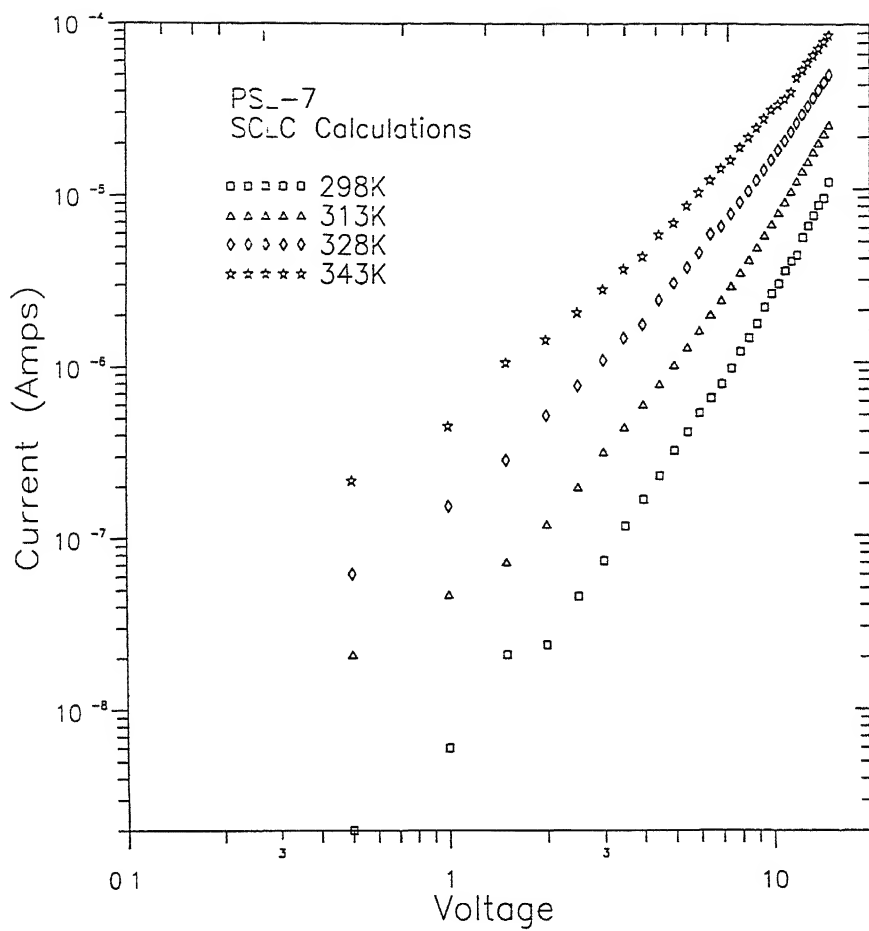


Fig 4.18 Bilogarithmic plot for SCLC fit for PSL-7.

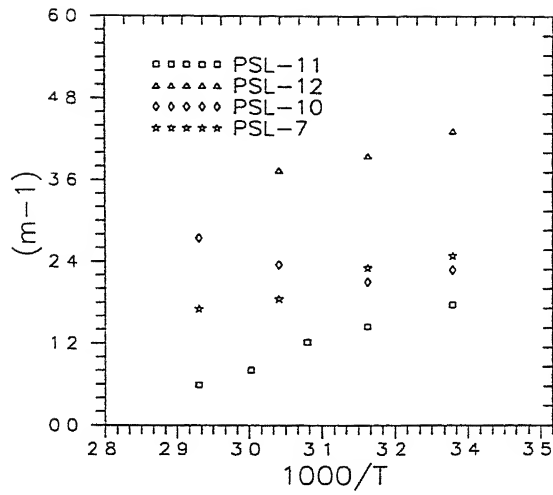


Fig 4.19 $(m-1)$ vs $1/T$ plot for SCLC fit
Non-linear dependence negates the exponential energy-trap distribution at Fermi-level

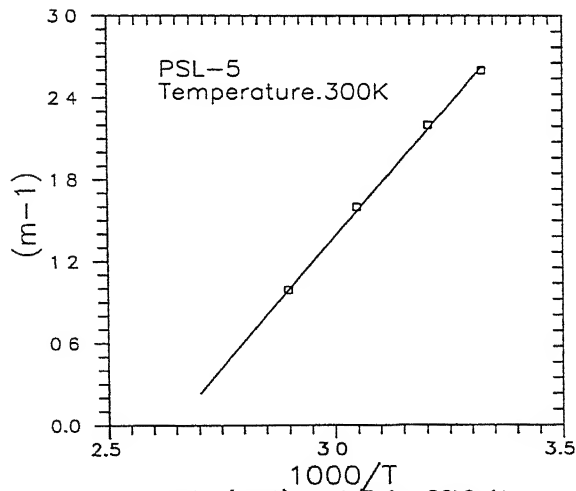


Fig 4.20 $(m-1)$ vs $1/T$ for SCLC fit
for PSL-5. The straight line fitted
to the data does not pass through
origin

are a menagerie of scattered points not following any particular regular curve. We, therefore, conclude from here that the energy-trap distribution is not exponential. 12 illustrated in Chapter 3, we employ here the method proposed by denBoer[45]. Even at voltages well within the super-Ohmic region, Fermi-level does not shift significantly ($\Delta E_f = 1 - \frac{12}{9} meV$) for voltage steps as large as 3V. The density of states (DOS) is of the order of $10^{16} eV^{-1} cm^{-3}$. The DOS values as also the Fermi-level shifts for various samples are given in Table 4.4.

Table 4.4
DOS function $g(E)$ and quasi Fermi-level shift (ΔE_f)

Sample	$g(E)$ and ΔE_f		
	$\Delta V = 1V$ ΔE_f meV; $g(E)$ $eV^{-1}cm^{-3}$	$\Delta V = 2V$ ΔE_f meV; $g(E)$ $eV^{-1}cm^{-3}$	$\Delta V = 3V$ ΔE_f meV; $g(E)$ $eV^{-1}cm^{-3}$
PSL-5	7; 7.2×10^{17}	8; 7.6×10^{17}	9; 7.3×10^{17}
PSL-7	6; 5.7×10^{17}	9; 6.2×10^{17}	10; 5.5×10^{17}
PSL-9	4; 7.5×10^{17}	9; 7.3×10^{17}	12; 8.1×10^{17}
PSL-10	2; 1.1×10^{18}	4; 5.5×10^{17}	8; 3.4×10^{17}
PSL-11	3; 1.1×10^{18}	6; 1.0×10^{18}	9; 1.0×10^{18}
PSL-12	5; 6.5×10^{17}	10; 6.3×10^{17}	12; 6.2×10^{16}

Nespurek et al[43] have devised a technique for finding the DOS distribution (see §3.1.2). From the plots of current activation energy E_a , calculated using equation 3.3, versus voltage in super-Ohmic region we can fit the DOS distribution as the form of the plot depends upon it. One such plot for PSL-7 is shown in Fig. 4.21

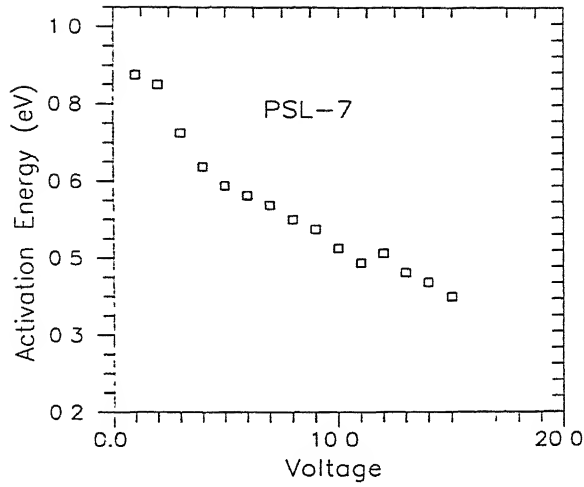


Fig 4.21 Voltage dependence of current activation energy obtained from SCLC fit for PSL-7

comparing it with that for exponential DOS distribution and that for discrete traps (as obtained by Nespurek et al), we conclude that the energy-trap distribution is not exponential nor it is a case of discrete trap states in the band gap. A detailed theoretical computation involving an appropriate DOS distribution fit coupled with the corresponding calculations on the experimental I-V data can fix up the problem but that is beyond the scope of this work.

4.2.4 AC Response of PS films

Conductivity

We have seen in the ac conductance versus frequency plots (cf. §4.2) that conductance follows a power law dependence $\sigma(\omega) \sim \omega^s$ with the exponent s having different values in two frequency ranges. The critical frequency demarcating the two frequency ranges depends upon the preparation conditions of the sample. In low frequency

range, $s \simeq 0.5$ while it is ~ 1 at higher frequencies. In homogeneous disordered systems there is only one crossover from a frequency independent conductivity (the dc value) to an ω^s regime with $s \simeq 0.8 - 0.9$. In PS, however, two crossovers are observed: dc to $\omega^{1/2}$ and $\omega^{1/2}$ to ω . This observation is in agreement with that of Ben-Chorin et al[37]. On the basis of weak temperature dependence of ac conductivity at higher frequencies and strong temperature dependence at low frequencies, they conclude that ac conductivity is caused by hopping of charge carriers in the vicinity of Fermi-level. This is more plausible explanation as compared to attributing the ac conductivity to polarisation of atoms or metallic particles. The electrons perform random walk in the disordered fractal system in the presence of the electric field. They pass a certain distance before the field changes its polarity.

For higher frequencies, a shorter distance is covered. In homogeneous systems, only one typical length scale exists, viz., average hopping length. In PS, two typical length scales are identified: the hopping length which is comparable to the typical crystallite size and the correlation length, which is the typical scale of inhomogeneity. This is the most probable reason for the two observed transitions. These two length scales are also observed in small angle X-ray scattering [49, 50]. In these experiments, a fractal structure is observed for length scales between a few hundreds of Å and upto 1000 Å. This is, however, a qualitative analysis only. The conductivity data at higher frequencies yield density of states at Fermi-level. This calculation is performed using equation 3.15.

The random walk dimension d_W can be determined directly from the frequency dependence of ac conductance using equation $s = 1 - 2/d_W$.

Table 4.5. Parameters calculated from ac conductivity data

Sample Name	s	d_W	\bar{d}/\tilde{d}	$g(E)(eV^{-1}cm^{-3})$
PSL-5	0.38	3.22	1.61	8.61×10^{18}
PSL-7	0.52	4.16	2.08	2.51×10^{16}
PSL-8	0.32	2.94	1.47	3.45×10^{19}
PSL-9	0.51	4.08	2.04	5.25×10^{17}

Table 4.5 lists the random walk dimensions for four typical samples. Keeping in mind the preparation conditions of samples as given in Table 4.1, we see a variation in the random walk dimension with both the etching current and the etching time. As our samples are insufficient in number, we do not perceive any specific trend in it. Since $d_W = 2\bar{d}/\tilde{d}$, a value of d_W gives a relation between the spectral (\bar{d}) and fractal (\tilde{d}) dimensions. In fractal materials, $\tilde{d} \geq 1.2$ [48]. It should be interesting to find \tilde{d} directly by inelastic neutron scattering in order to investigate whether this applies also to PS.

Capacitance-Frequency Behaviour

The most striking effect observed in PS (cf. §4.1) is the rapid fall of capacitance at lower frequencies and almost saturation at higher frequencies. The exact ranges of frequencies for a particular behaviour depends upon the preparation conditions of the sample. The divergence of capacitance (dielectric constant) at lower frequencies is usually attributed to contact polarisation known as Maxwell-Wagner phenomenon[34]. The parasitic capacitance of contacts leads to such a behaviour. It is known that the presence of contact polarisation leads to thickness dependence

of dielectric constant[56]. Although Ben-chorin et al[37] negate this idea, we find it difficult to compare any two samples of PS and then distinguish between them on the basis of thickness only. In the absence of a clear understanding of structural properties of PS as a function of preparation conditions, varying the thickness may mean to produce a different material altogether. Any variation in crystallite size leads to a different field distribution over the PS layer and this must change the dielectric constant. So Maxwell-Wagner polarisation cannot be negated outright. It may be concomitantly taking place while some unknown physical process prevails to create the effect.

Chapter 5

Summary and Conclusions

The present work deals with the carrier transport in porous silicon (PS) under the application of ac and dc fields. The PS layers used in these measurements were prepared by electrochemical etching of p (Boron) doped c-Si substrates with a dilute (20%) solution of HF and ethanol. The polished face ($[100] \pm 5$ deg orientation) of substrate was anodised. The preparation conditions were optimised for good visible photoluminescence (PL) of the PS layers so prepared. It was found that low etching currents ($\sim 5mA/cm^2$) as well as high etching currents ($\sim 70 - 80mA/cm^2$) do not yield luminescent PS layers. The etching times had no observable effect on the luminescence. This is explained as due to less porosity obtained with low etching currents and the presence of amorphous layer obtained at very high etching currents. Free-standing PS layers were also prepared using the same technique. In order to detach the PS layers from the substrate, the etching current was increased abruptly to electropolishing value ($\sim 500mA/cm^2$) at the end of the PS formation. The free-standing PS layers and c-Si supported PS layers were all luminescent and their luminescence could be observed with naked eye when illuminated by a 125W mercury lamp. The self-supporting films of PS were brittle and so fragile that no

contacts could be made on them for electrical measurements. Therefore, no electrical measurements have been performed on free-standing PS films.

For transport measurements, Al or NiCr dots of about 1mm dia were evaporated on PS layers in vacuum ($\sim 10^{-6}$ torr). In order to avoid the metal vapours from getting into the pores thereby reducing the effective thickness of porous layer, the sample was kept at about 60 deg with horizontal during contact evaporation. The current-voltage (I-V) characteristics are found to be similar in sandwich and coplanar geometries.

The I-V characteristics are measured in the temperature range $300K \leq T \leq 343K$. Some of samples have asymmetric while others have symmetric I-V characteristics with respect to the polarity of applied dc voltage. Conceptualising the Al-PS-Si trilayer as a combination of resistances (voltage-dependent) and non-Ohmic interfaces, we find that the current in the trilayer structure is controlled by contact properties in case of asymmetric I-V characteristics. This is supported by the fact that asymmetric I-V characteristics are found in less porous and very thin PS film, so that the resistance of the PS layer is much less than the resistance of contacts. When PS film is sufficiently porous ($> 50\%$) and thicker ($\geq 5\mu m$) so that the resistance of PS layer is much greater than that of the contacts, symmetric I-V characteristics are found. Another feature that is prominent in the I-V characteristics is the super-Ohmic behaviour at higher voltages and at higher temperatures. This behaviour is attributed to carrier transport controlled by either Poole-emission or by space charge limited currents (SCLC).

In Poole-Frenkel mechanism[42], the normal state of a dielectric material is viewed as a system of neutral atoms and having no free electrons. After thermal ionisation of an atom, the electron moves under the influence of the field of the remaining positive ion and tends to polarise the remaining neutral atoms thereby

reducing the ionisation energy. This energy is further reduced when an external field is applied. Analysis of data (Poole-Frenkel plot) yields the dc activation energy (ϕ_0) for Poole-Frenkel mechanism to be about 0.39–0.60eV, which is in agreement with that reported by Ben-Chorin et al[30]. However, some of our samples do not show any linear region in the Poole-Frenkel plot. Another test for Poole-Frenkel mechanism assertion is the consistency of the values of parameters obtained from the calculations based on it. We have calculated the dielectric constants (ϵ_r) from the Poole-Frenkel fit for our samples of PS layers. The typical values are found to be between 5 and 10. Ben-Chorin et al[30] report values of dielectric constant between 2.5 and 10. These values, however, do not reflect any physical property of PS and are therefore treated as fit parameters only. There can be no clear cut meaning of dielectric constant for the microscopic trapping level as it is obtained by employing shape-dependent effective medium averaging over regions of the order of few μm in optical experiments. For transport in Poole-Frenkel sense, a local electric field on the scale of few angstroms is relevant. These dimensions are comparable to crystallite sizes ($\sim 3\text{--}4\text{nm}$) reported for PS in the literature[32, 30] For such crystallites, the notion of dielectric constant does not apply[30].

The current injected by the metal (Al or NiCr) contact into the PS builds up a space charge region inside the porous layer. This resists further injection of carriers. Thus, the currents are limited by space charge. The I–V relationship is strongly influenced by the energy-trap distribution. To determine the DOS for trapping levels, we have applied the step by step method[44, 45]. This yields a density of states (DOS) value at the Fermi level in the range $10^{16} - 10^{18} eV^{-1} cm^{-3}$, for our samples with varying thickness and crystallite size. This is in agreement with the values reported by Ben-Chorin et al[37].

ac conductivity measurements were performed on PS layers by measuring admit-

tance in the frequency range 5Hz to 10MHz. From this, capacitance and conductance were calculated. The frequency of capacitance yields the frequency dependence of dielectric constant. It is found that dielectric constant falls rapidly at lower frequency range and almost saturates at higher frequencies. A bilogarithmic plot of conductance vs frequency exhibits two linear regions. In the lower frequency region (5Hz – 5kHz) the exponent s in $\sigma(\omega) \sim \omega^s$ is very near to 0.5 and at higher frequencies, it is about 0.80. The exponent value of $s \simeq 0.5$ is explained by the carrier transport controlled by fractal structure of PS layers[37]. The value of exponent is limited by the random walk dimension which is the distance covered by a carrier on an average between any two consecutive reversals of polarity of the applied ac field. The random walk dimension calculated for our samples are reasonably consistent with each other (see Table 4.6). At higher frequencies, the $\omega^{0.8}$ dependence of conductance has been explained by ac transport at Fermi level[37]. The density of states (DOS) at the Fermi level is found to be in the range $10^{17} - 10^{19} eV^{-1} cm^{-3}$. We find that DOS at Fermi level calculated from ac conductivity measurements agrees with that calculated from dc conductivity measurements.

5.1 Scope for Future Work

We find that our results can be explained by the Poole-Frenkel as well as the SCLC mechanism for the carrier transport in PS. Therefore, more work needs to be done for deciding which one of the two mechanisms is really operative in PS. This is difficult for various reasons. Firstly, the nature of contacts on the PS layers is not quite clear. Also, the preparation techniques need to be evolved to obtain truly Ohmic contacts. Some unknown modification at the interface between the porous layer and the metal film by the penetration of metal contacts and the admixtures

present unavoidably also change the measured properties. Bad contacts not only mar the prospect of best dc results but also the ac results defy any interpretation due to contact polarisation and capacitive effects originating therefrom. Further, in order to eliminate the substrate effects transport measurements on free-standing PS films are desirable.

Next, other conduction mechanism should also be considered. Hopping of carriers around Fermi level is hinted at by Ben-Chorin et al[37] and further supported by Kocka et al[41]. This needs to be explored by more experiments. Combined ac and dc conductivity measurements at different temperatures can yield an assertive information in this regard. Moreover, the ac conductivity measurements on PS layers can relate the morphology of PS layers to the transport properties. The density of states at Fermi level has been obtained in our experiments. However, the distribution of these states has not been found. Detailed theoretical calculations coupled with SCLC measurements are a handy tool to model an energy-trap distribution at the Fermi level[43]. Further, we found that our freshly prepared PS layers have PL are photoconductive, but lose their PL and photoconductivity upon ageing, as observed by other workers as well[57]. A study of transport in PS as function of ageing would therefore be of much interest, as it may ~~and it may~~ shed light on the suitability of this material for device applications.

Bibliography

- [1] A. Uhler. *Bell Syst. Tech. J.*, **35**, 333(1956).
- [2] L.T. Canham. *Appl.Phys.Lett.*, **57**, 1046(1990).
- [3] R. E. Hummel and S. S. Chang. *Appl. Phys. Lett.*, **61**, 1965(1992).
- [4] D. Ruter, T. Kunze, and W. Bauhofer. *Appl. Phys. Lett.*, **64**, 3006(1994).
- [5] K. W. Cheah and C. H. Choy. *Solid State Commun.*, **91**, 795(1994).
- [6] N. Noguchi and I. Suemune. *Appl. Phys. Lett.*, **62**, 1429(1993).
- [7] S. Banerjee. *Bull.Mater.Sci.*, **17**, 533(1994).
- [8] Y. Kanemitsu. *Phys. Rev. B*, **48**, 12357(1993).
- [9] J. R. Haynes and W. C. Westphal. *Phys. Rev.*, **101**, 1676(1956).
- [10] W. Michaels and M. H. Pilkuhn. *Physica Status Solidi*. **36**, 311(1969).
- [11] G. Di Francia, P. Maddalena, and D. Ninno. *Solid State Commun.*, **96**, 579(1995).
- [12] Hideki Koyama, Minoru Araki, Yuko Yamamoto, and Nobuyoshi Koshida. *Jpn. J. Appl. Phys.*, **30(12B)**, 3606(1991).

- [13] J C.Vial, A.Bsiesy, F.Gaspard, R.Herino, M.Ligeon, F.Moller, R.Romenstain. and R.M.Macfarlane. *Phys.Rev.*, **45**, 14171(1992).
- [14] M. I. J. Beale, J. Benjamin, M. J. Uren, N. G. Chew, and A. G. Cullis. *J. Cryst. Growth*, **73**, 622(1985).
- [15] M.S. Brandt, H.D. Fuchs, M. Strutzmann, J. Weber, and M. Cardona. *Solid State Commun.*, **81**, 307(1992).
- [16] A. G. Cullis and L. T. Canham. *Nature*, **353**, 335(1991).
- [17] D. J. DiMaria, J. R. Kirtley, E. J. Pakulis, D. W. Dong, T. S. Kuan, F. L. Pesavento, T. N. Theis, J. A. Kutro, and S. D. Brorson. *J. Appl. Phys.*, **56**, 4011(1984).
- [18] S. Furukawa and T. Miyasato. *Phys. Rev. B*, **38**, 5726(1988).
- [19] S. Furukawa and T. Mijasato. *Phys. Rev. B*, **38**, 5726(1988).
- [20] H. Takagi, H. Ogawa, Y. Yamazaki, A. Ishizaki, and T. Nakagiri. *Appl. Phys. Lett.*, **56**, 2379(1990).
- [21] F. Kozlowski, V. Petrova Koch, A. Kux, W. Stadler, A. Fleischmann, and H. Sigmund. *J. Non-Cryst. Solids*, **137/138**, 91(1991).
- [22] S.M. Prokes, O.J. Glembocki, V.M. Bermudez, R. Kaplan, L.E. Friedersdorf, and P.C. Searson. *Phys.Rev.B*, **45**, 13788(1992).
- [23] C. Tsai, K. H. Li, D. S. Kinosky, R. Z. Qian, T. C. Hsu, J. T. Irby, S. K. Banerjee, A. F. Tasch, J. C. Campbell, B. K. Hance, and J. M. White. *Appl. Phys. Lett.*, **60**, 1700(1992).

- [24] A. Halimaoui, C. Oules, G. Bomchil, A. Bsiesy, F. Gaspard, R. Herino, M. Ligeon, and F. Muller. *Appl. Phys. Lett.*, **59**, 304(1991).
- [25] N. Koshida and H. Koyama. *Appl. Phys. Lett.*, **60**, 347(1992).
- [26] P. Steiner, F. Kozlowski, and W. Lang. *Appl. Phys. Lett.*, **62**, 2700(1993).
- [27] N. Koshida, H. Koyama, Z. Yamamoto, and G. J. Collins. *Appl. Phys. Lett.*, **63**, 2655(1993).
- [28] J. Kocka, A. Fejfar, and I. Pelant. *Phys. Stat. Sol. (b)*, **190**, 27(1995).
- [29] C. Cadet, D. Deresmes, D. Vuillaume, and D. Stievenard. *Appl. Phys. Lett.*, **64**, 2827(1994).
- [30] M. Ben-Chorin, F. Moller, and F. Koch. *Phys. Rev. B*, **49**, 2981(1994).
- [31] P. Hlinomaz, O. Klima, A. Hospodkova, E. Hulicius, J. Oswald, E. Sipek, and J. Kocka. *Appl. Phys. Lett.*, **64**, 3118(1994).
- [32] A. Fejfar, I. Pelant, E. Sipek, J. Kocka, G. Juska, T. Matsumoto, and Y. Kanemitsu. *Appl. Phys. Lett.*, **66**, 1098(1995).
- [33] A. Diligenti, A. Nannini, G. Pennelli, and F. Pieri. *Appl. Phys. Lett.*, **68**, 687(1996).
- [34] A. K. Jonscher. *Nature*, **267**, 673(1979).
- [35] A. R. Long. *Adv. Phys.*, **31**, 553(1982).
- [36] J. R. Macdonald. *Impedance Spectroscopy*. John Wiley & Sons, New York, 1987.

- [37] M.Ben-Chorin, F.Moller, F.Koch, W.Schirmacher, and M.Eberhard. *Phys.Rev.*, **51**, 2199(1995).
- [38] R. L. Smith and S. D. Collins. *J. Appl. Phys.*, **7**, R1(1992).
- [39] W. H. Lee and Choochon Lee. In *16th International Conference on Amorphous Semiconductors-Science and Technology*, Kobe (Japan), September 4–9, 1995.
- [40] Y. Lubianiker, I. Balberg, E. Fefer, and Y. Shapira. In *16th International Conference on Amorphous Semiconductors- Science and Technology*, Kobe (Japan), September 4–9, 1995.
- [41] J. Kocka. I. Pelant, and A. Fejfar. In *16th International Conference on Amorphous Semiconductors- Science and Technology*, Kobe (Japan), September 4–9, 1995.
- [42] J.Frenkel. *Phys.Rev.*, **54**, 647(1938).
- [43] S. Nespurek. O. Zmeskal, and F. Schauer. *Phys. Stat. Sol. (a)*, **85**, 619(1984).
- [44] D. S. Misra, A. Kumar, and S. C. Agarwal. *J. Non-Cryst. Solids*, **76**, 215(1985).
- [45] W. denBoer. *J. Phys. (Paris)*, **42**, C4(1981).
- [46] N. F. Mott and E. A. Davis. *Electronic Processes in non-crystalline materials*. International Series of monographs on Physics. Clarendon Press, Oxford, 2nd edition, 1979.
- [47] J. P. Clerc, G. Giraud, M. M. Laugier, and J. M. Luck. *Adv. Phys.*, **39**, 191(1990).
- [48] B. B. Mandelbrot. *The Fractal Geometry of Nature*. Freeman, New York, 1977.

- [49] P. Goudeau, A. Naudon, G. Bomchil. and R. Herino. *J. Appl. Phys.*, **66**, 625(1989).
- [50] V. Vezin, P. Godeau, A. Naudon, A. Halimaoui, and G. Bomchil. *Appl. Phys. Lett.*, **60**, 2625(1992).
- [51] T. Nakayama, K. Yakubo, and R. L. Orbach. *Rev. Mod. Phys.*, **66**, 381(1994).
- [52] Y. Gefen, A. Aharony, and S. Alexander. *Phys. Rev. Lett.*, **50**, 77(1983).
- [53] George C. John and V. A. Singh. *Physics Reports*, **263**, 93(1995).
- [54] S. M. Sze. *Physics of Semiconductor Devices*. Wiley Eastern Limited, New Delhi, 2nd edition, 1981.
- [55] D. M. Pai. *J. Appl. Phys.*, **46**, 5122(1975).
- [56] J. Kocka and J. Kristofic. *Phys. Status Solidi A*, **45**, 559(1978).
- [57] Suk-Ho Choi, Haeyang Chung, and Gyu-Seung Shin. *Solid State Commun.*, **95**, 341(1995).